Computed imaging: how physics connects external measurements to internal structure

P Scott Carney

Beckman Institute for Advanced Science and Technology
Department of Electrical and Computer Engineering
University of Illinois at Urbana-Champaign

U Toronto 2 October 2008

Acknowledgements

Prof. P. Scott Carney

OSG Optical Science Group

Post-Doctoral Fellows

Brynmor Davis

Graduate Students

Jin Sun (PhD 2008)

http://optics.beckman.uiuc.edu

The National Science Foundation, NASA, USAF, Beckman Foundation

Acknowledgements:
ISAM

Prof. Stephen A. Boppart

BIOPHOTONICS IMAGING LABORATORY

Graduate Students	**Post-Doctoral Fellows**
Tyler Ralston	**Dan Marks**
Adam Zysk	

Acknowledgements: NFOT

- John Schotland (U Penn)
- Vadim Markel (U Penn)
- Rich Frazin (U Mich)
- Sergey Bozhvolnyi (U Aalborg)

Inverse problems

RADAR

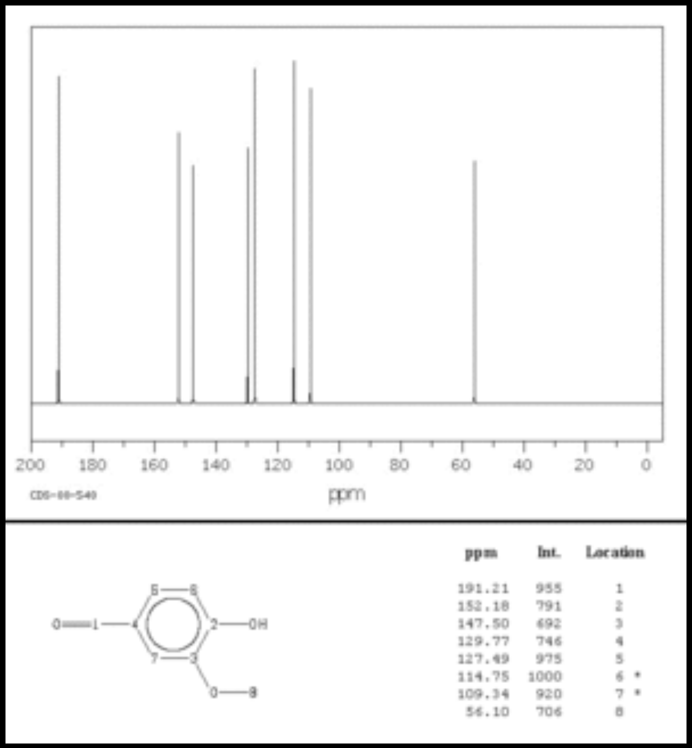

NMR spectroscopy

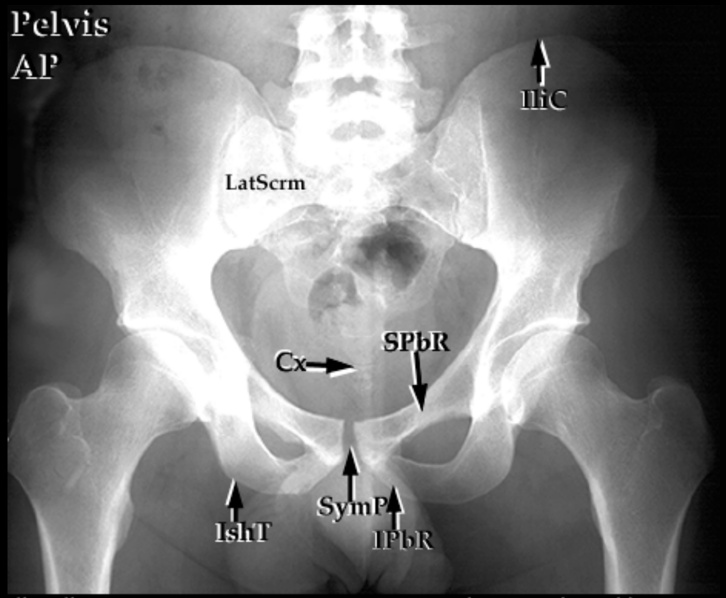

IliC=Iliac Crest
LatScrm=Lateral Sacrum
Cx=Coccyx
IshT=Ischial Tuberosity

SPbR=Superior Pubic Ramus
SymP=Symphysis Pubis
IPbR=Inferior Pubic Ramus

X-ray projection

Optical Coherence Tomography
*Spectral Domain

Inverse problems

RADAR

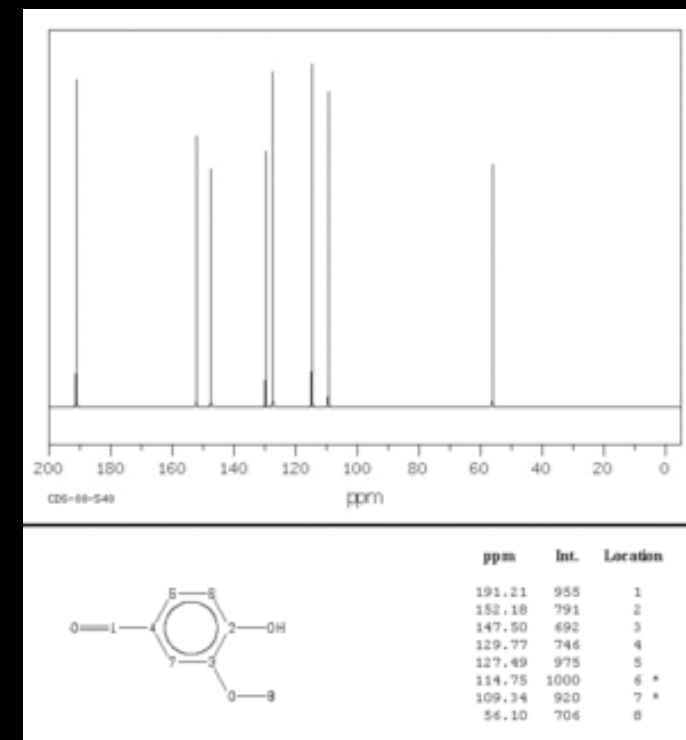

NMR spectroscopy

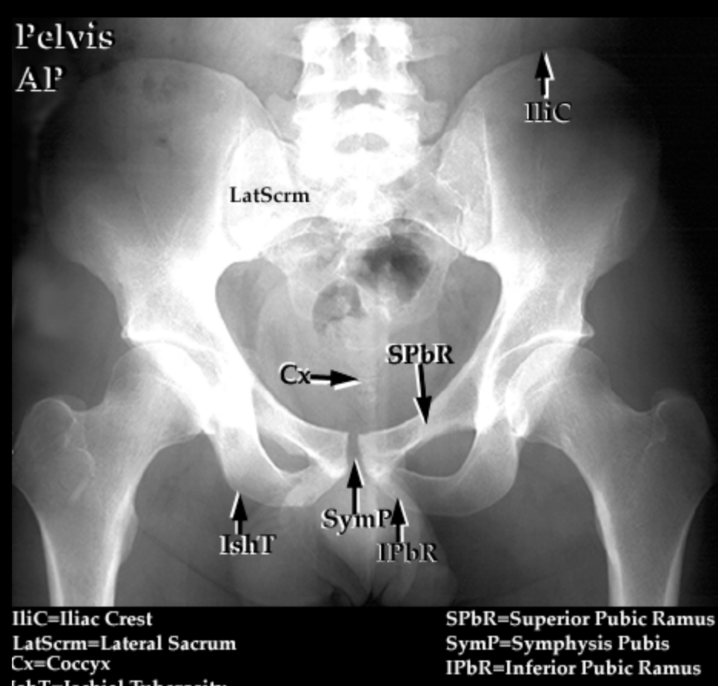

X-ray projection

Optical Coherence Tomography
*Spectral Domain

Inverse problems

Synthetic Aperture Radar
*Rob Morrison

Magnetic Resonance Imaging
*Ian Atkinson

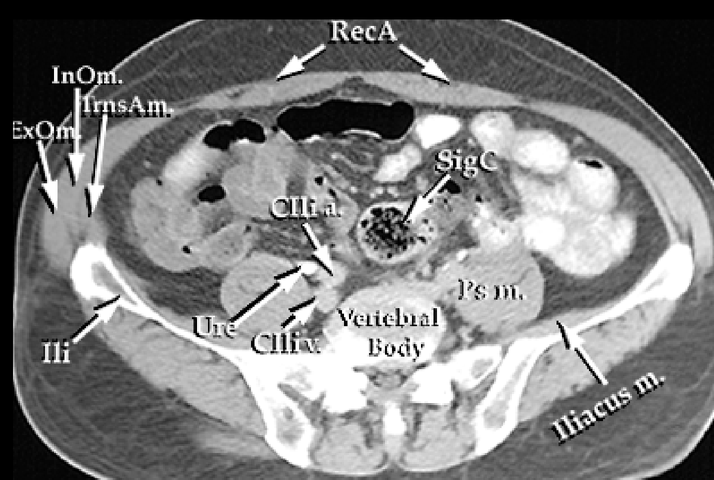

CT

Optical Coherence Tomography
*Spectral Domain

Shadowgrams to structure

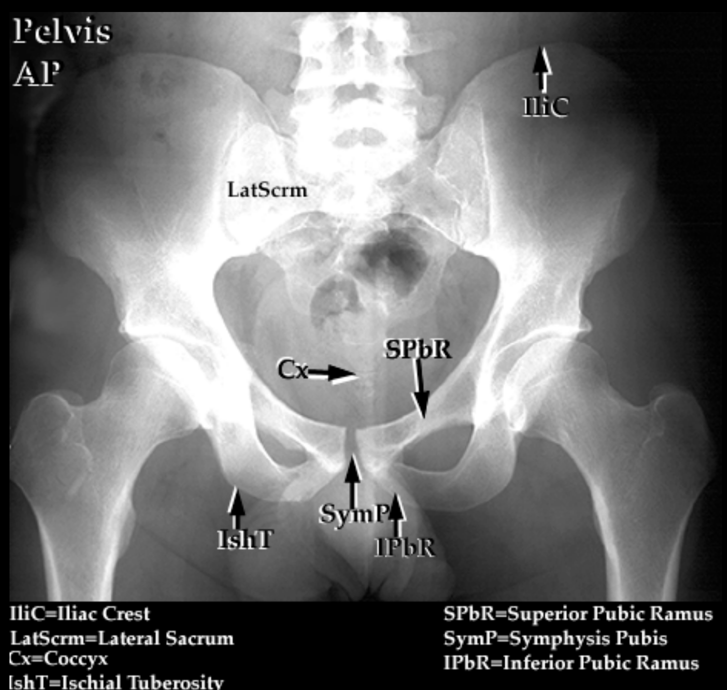

X-ray projection

Physics

$$I(P) = I(P_0)e^{-\int_{P_0}^{P} \alpha(\mathbf{r})dl}$$

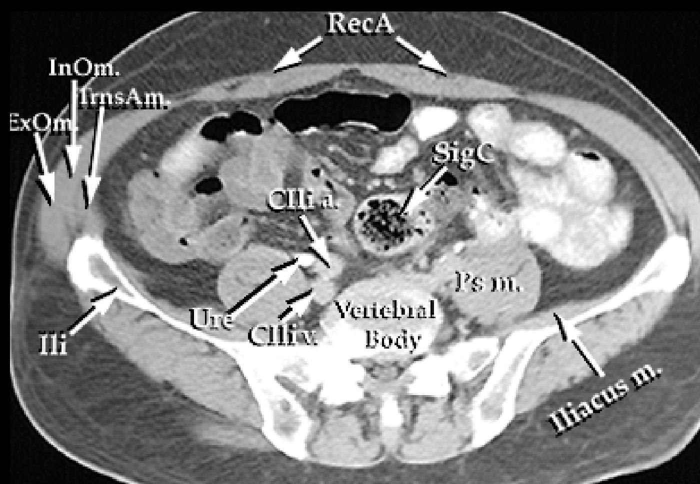

CT

Maxwell Eq. → Geometrical Optics → Beers law

Spectra to structure

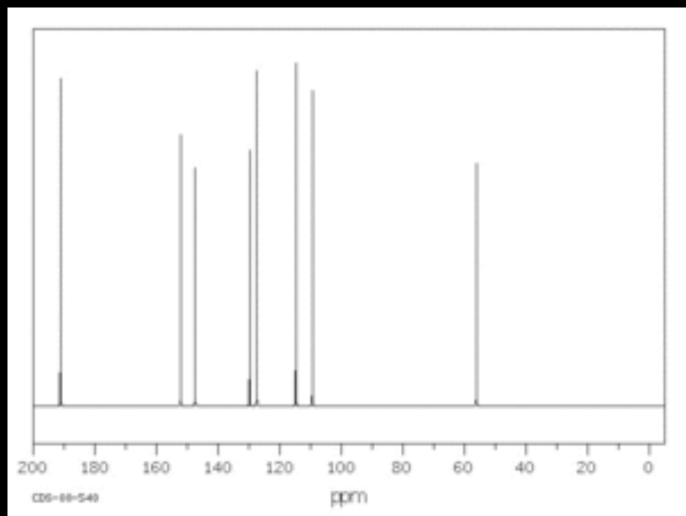

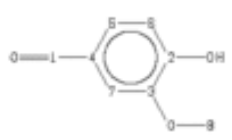

ppm	Int.	Location
191.21	955	1
152.18	791	2
147.50	692	3
129.77	746	4
127.49	975	5
114.75	1000	6 *
109.34	920	7 *
56.10	706	8

NMR spectroscopy

Physics

$$\omega = 2B\mu/\hbar$$

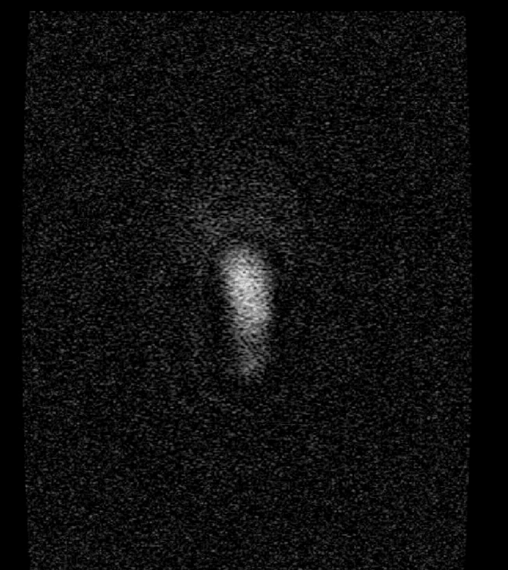

Maxwell Eq. + Q.M. w/ spin → Larmor freq.

+ Stat mech. → τ_1 , τ_2

Echograms to structure

RADAR

Physics

Synthetic Aperture Radar
*Rob Morrison

$$S(\mathbf{r},\omega) = A(\omega)\int d^3r'\ h(\mathbf{r}'-\mathbf{r},\omega)\eta(\mathbf{r})$$

Maxwell Eq. + Reflectance → Stolt mapping

Optical Coherence Tomography: range finding with low-coherence interferometry

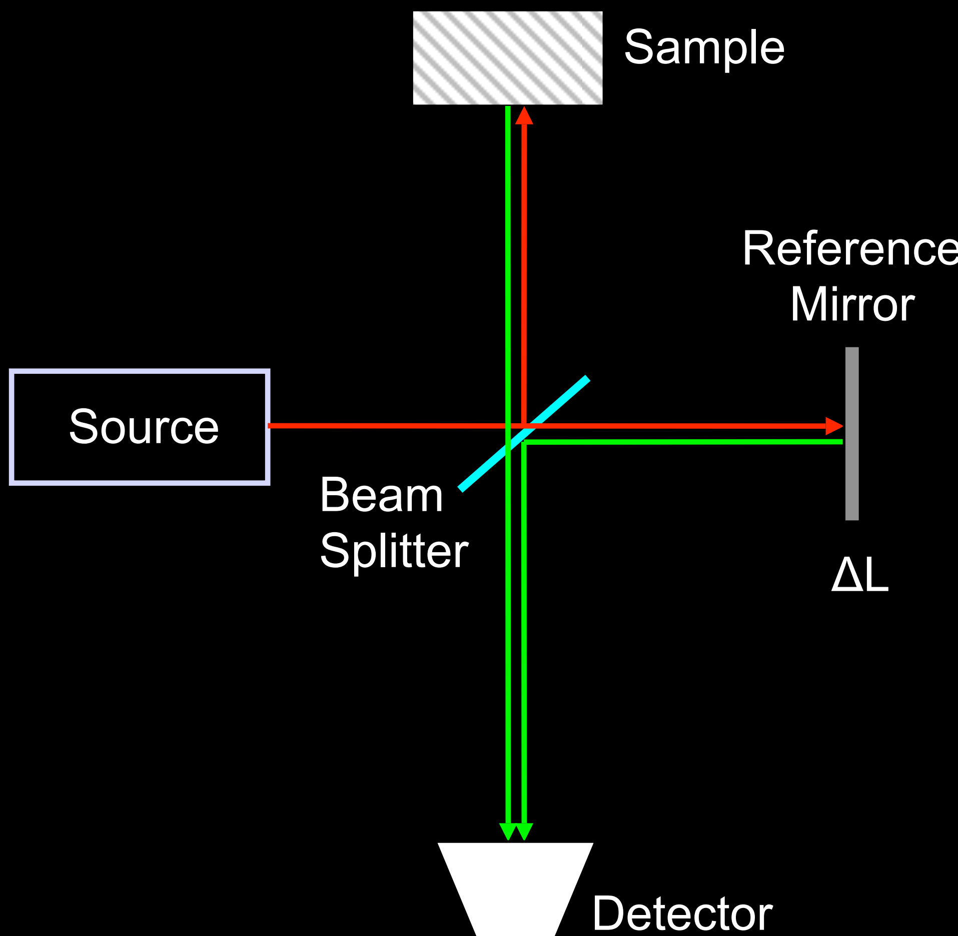

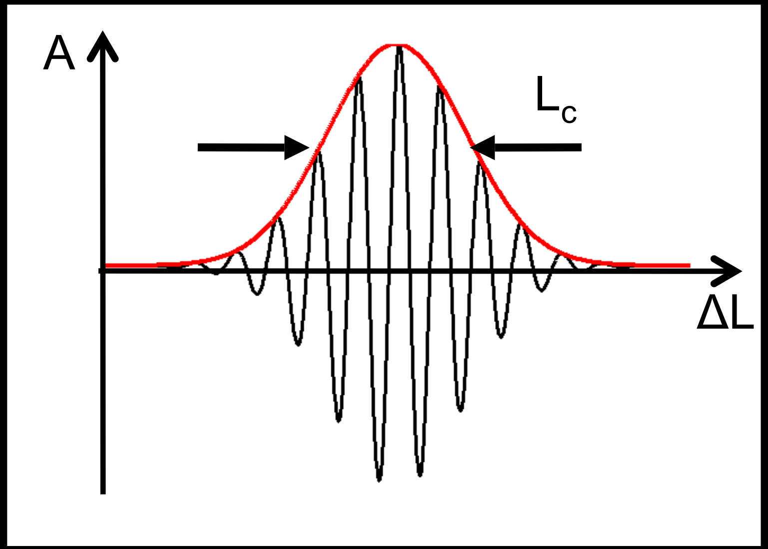

Signal processing: speckle reduction, numerical dispersion correction

Transverse scanning in OCT imaging

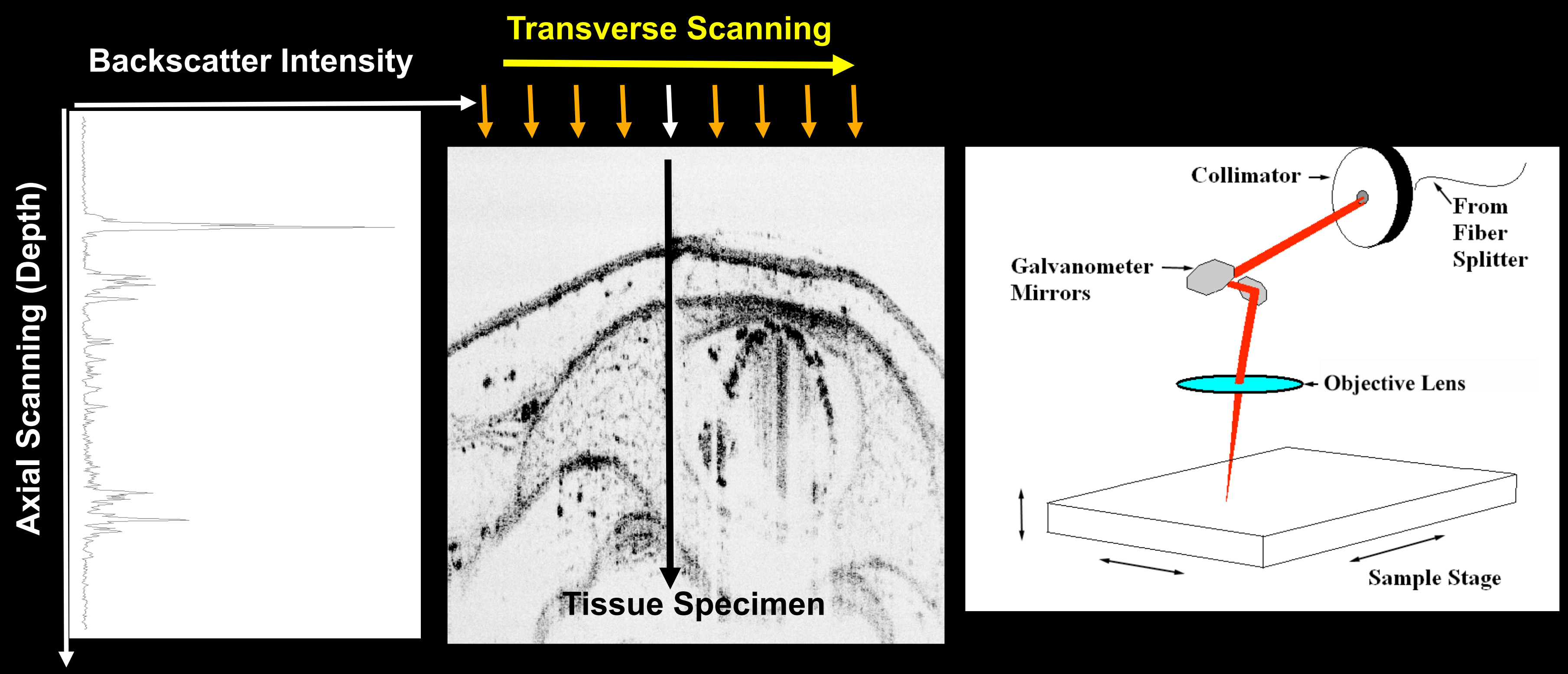

OCT *vs* histology - human tumor

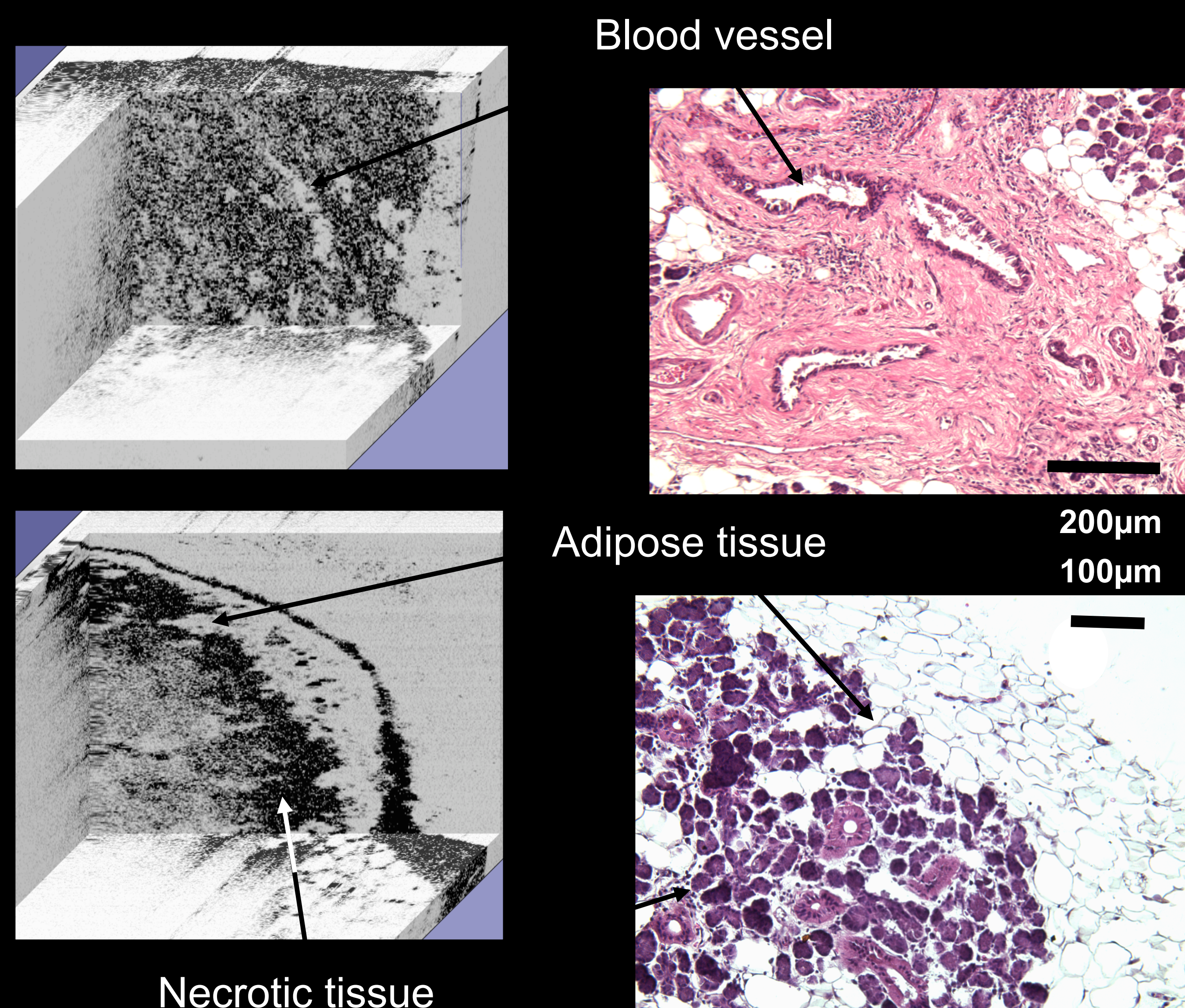

Luo W, Nguyen FT, Zysk AM, Ralston TS, Brockenbrough J, Marks DL, Oldenburg AL, Boppart SA, “Optical Biopsy of Lymph Node Morphology using Optical Coherence Tomography.” Technology in Cancer Research and Treatment, 4 (5), 539-547, October 2005.

The problem

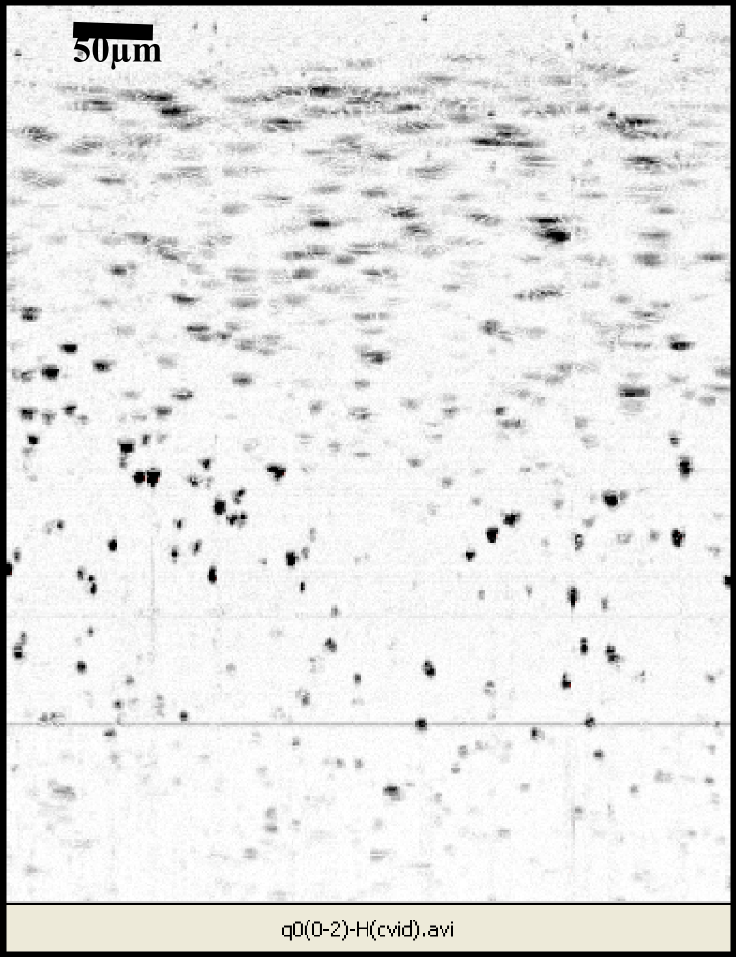

Beam Focusing

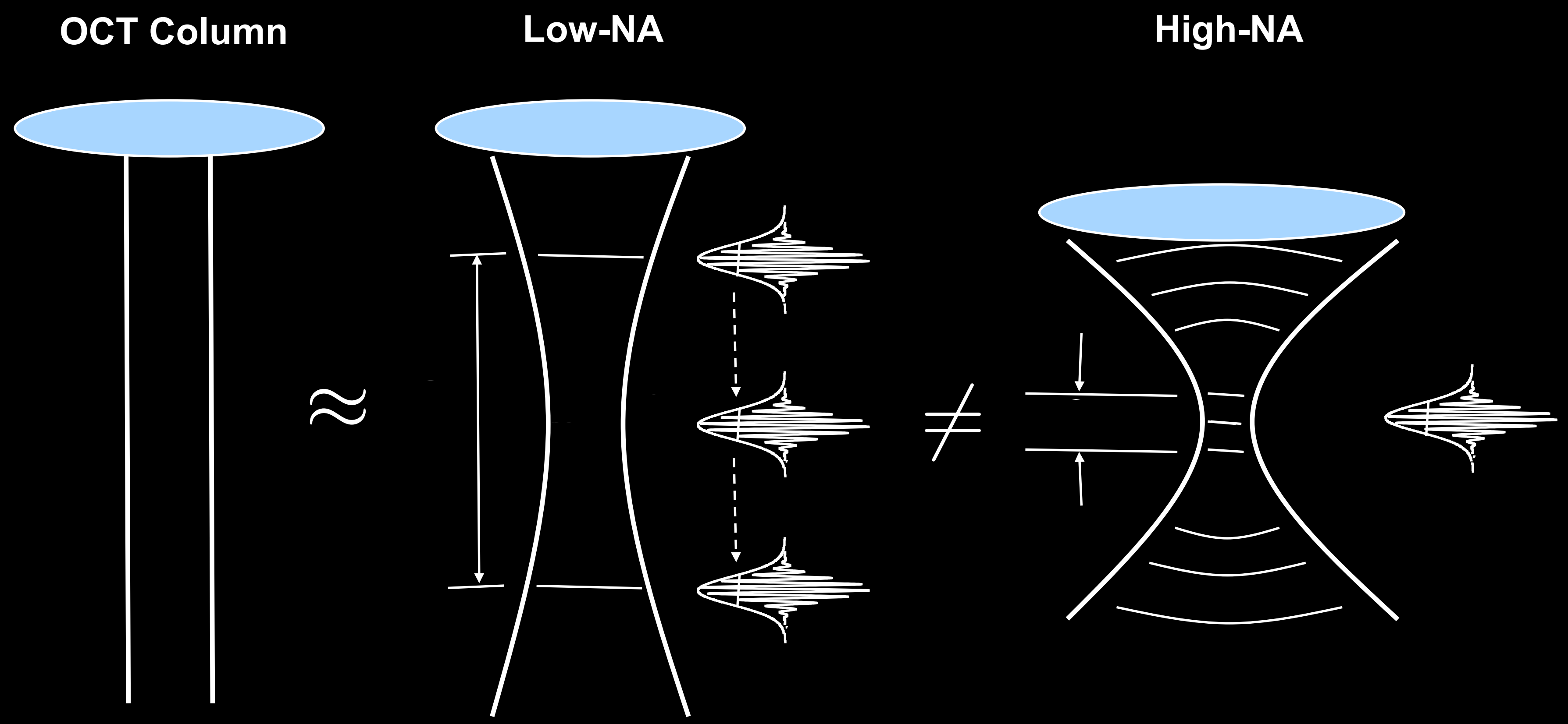

B. Hermann, *et.al.,* "Adaptive-optics ultrahigh-resolution optical coherence tomography," Opt. Let., vol. 29, pp. 2142-2144, 2004.

W. Drexler *et. al.*, "*In vivo* ultrahigh-resolution optical coherence tomography," Opt. Let. Vol.24 No.17 pp. 1221-1223

Spectral domain OCT: all the data at once

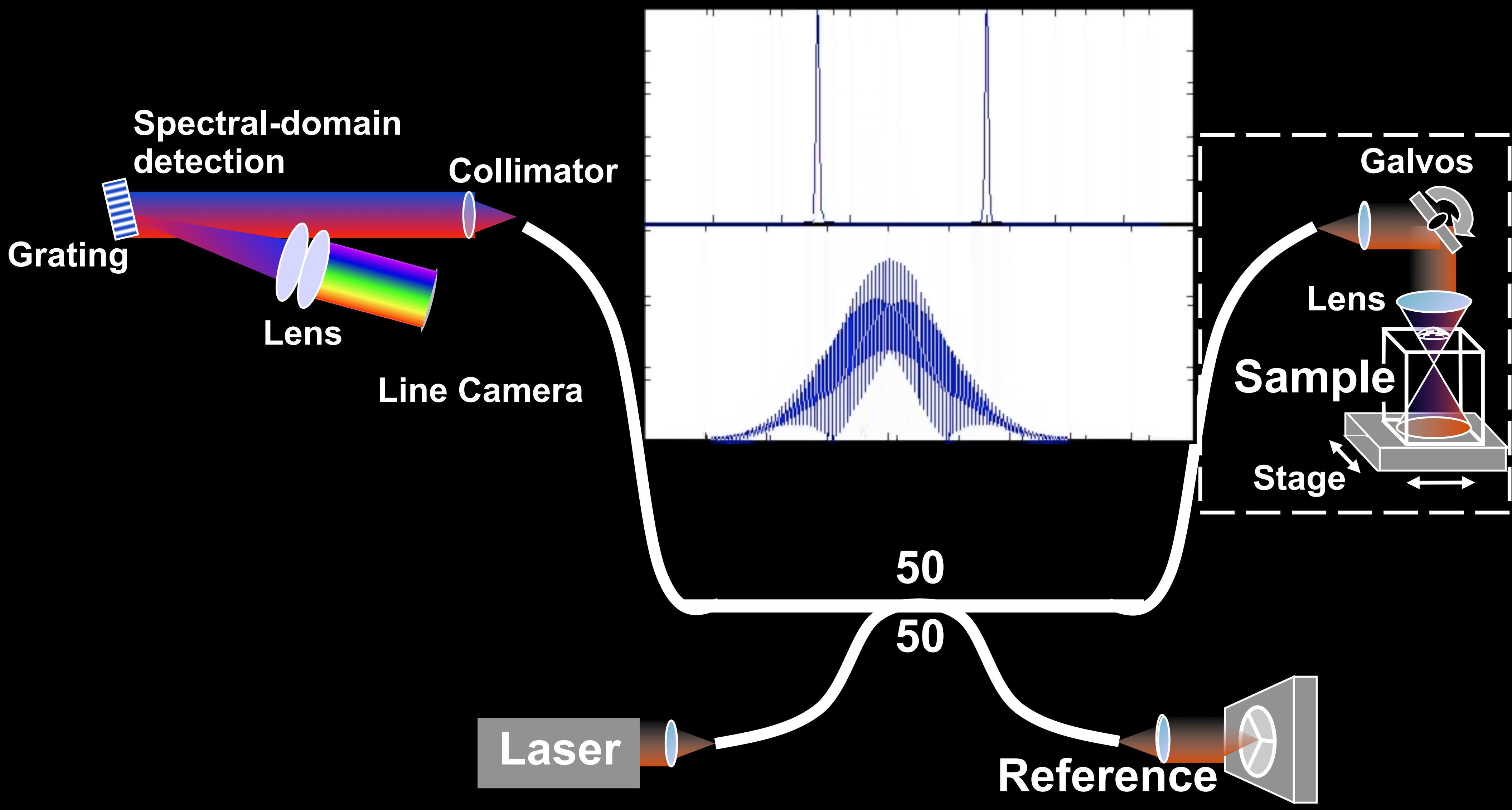

Strategy

- Develop forward model for illumination, light-sample interaction, and detection
- Linearize in the sample if possible
- Simulate and compare forward data to reality
- Apply appropriate approximations
- Invert, analytically if possible

Mathematics

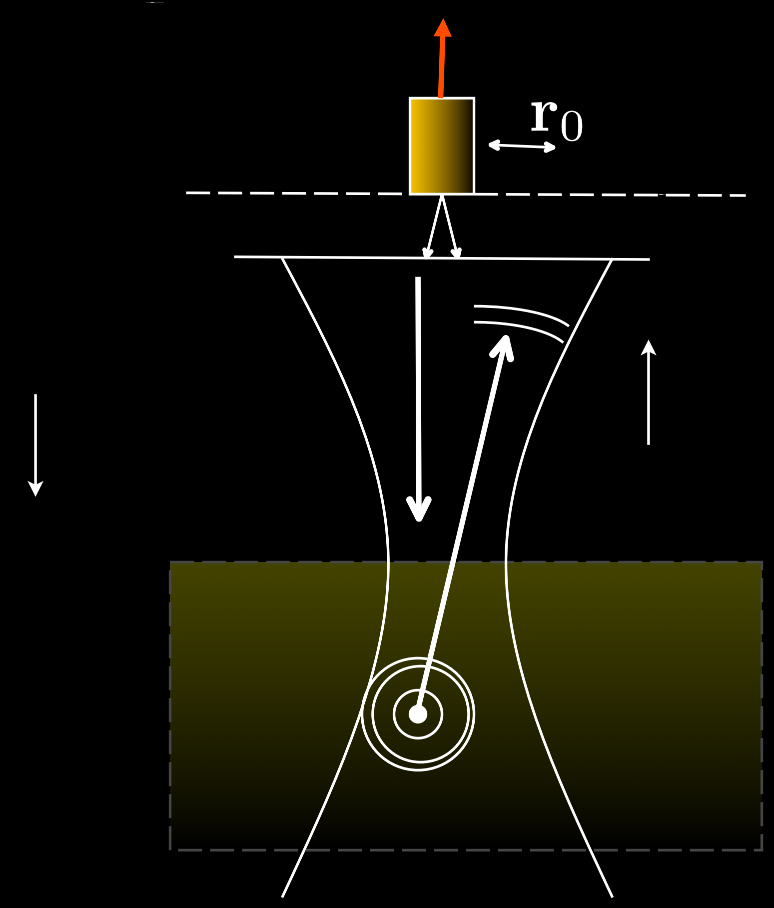

Mathematics

$$U_i(\mathbf{r}, \mathbf{r}_0, k) = A(k) g(\mathbf{r} - \mathbf{r}_0)$$

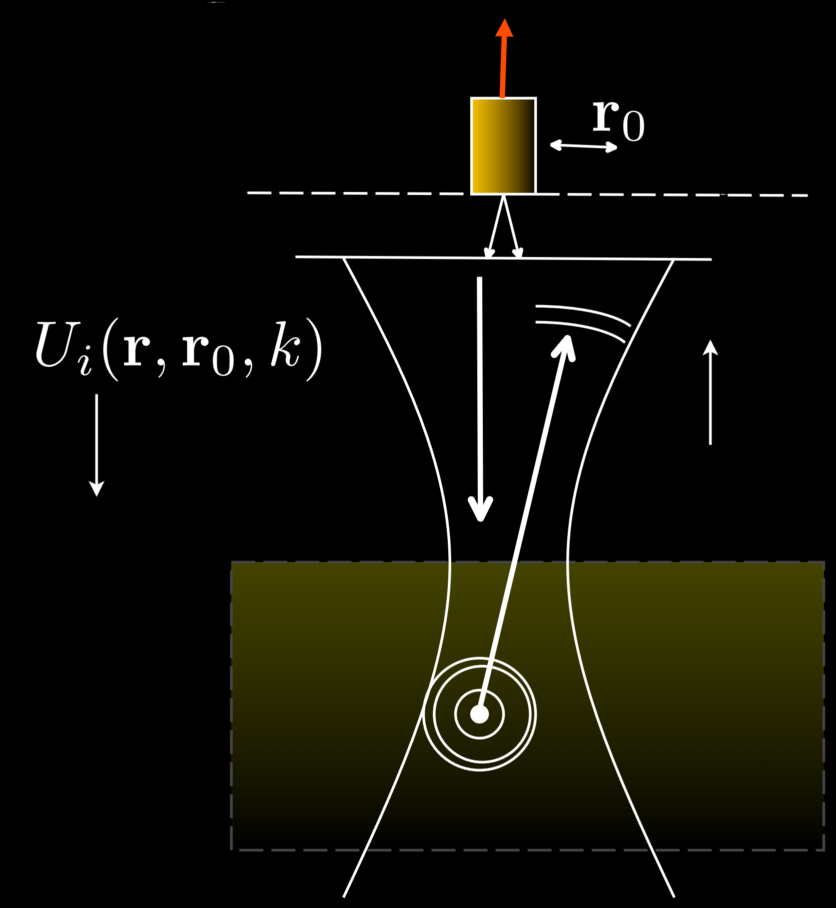

Mathematics

$$U_i(\mathbf{r}, \mathbf{r}_0, k) = A(k) g(\mathbf{r} - \mathbf{r}_0)$$

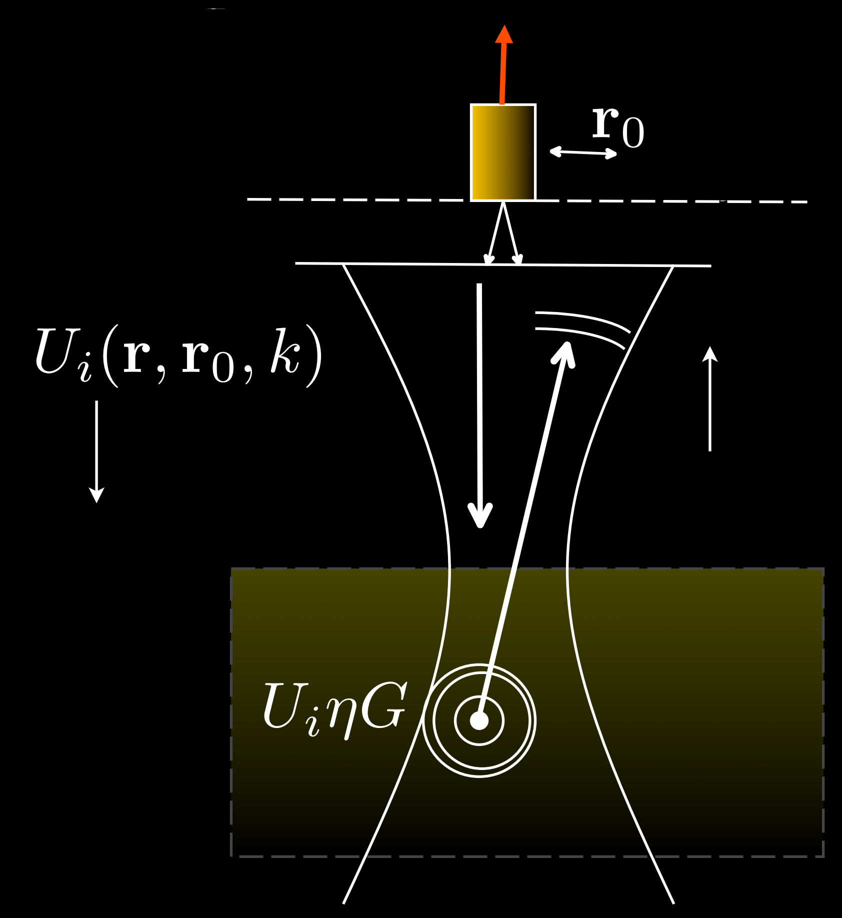

Mathematics

$$U_i(\mathbf{r}, \mathbf{r}_0, k) = A(k) g(\mathbf{r} - \mathbf{r}_0)$$

$$U_s(\mathbf{r}, \mathbf{r}_0, k) = \int d^3 r' \, G(\mathbf{r}', \mathbf{r}, k) \eta(\mathbf{r}') U_i(\mathbf{r}', \mathbf{r}_0, k)$$

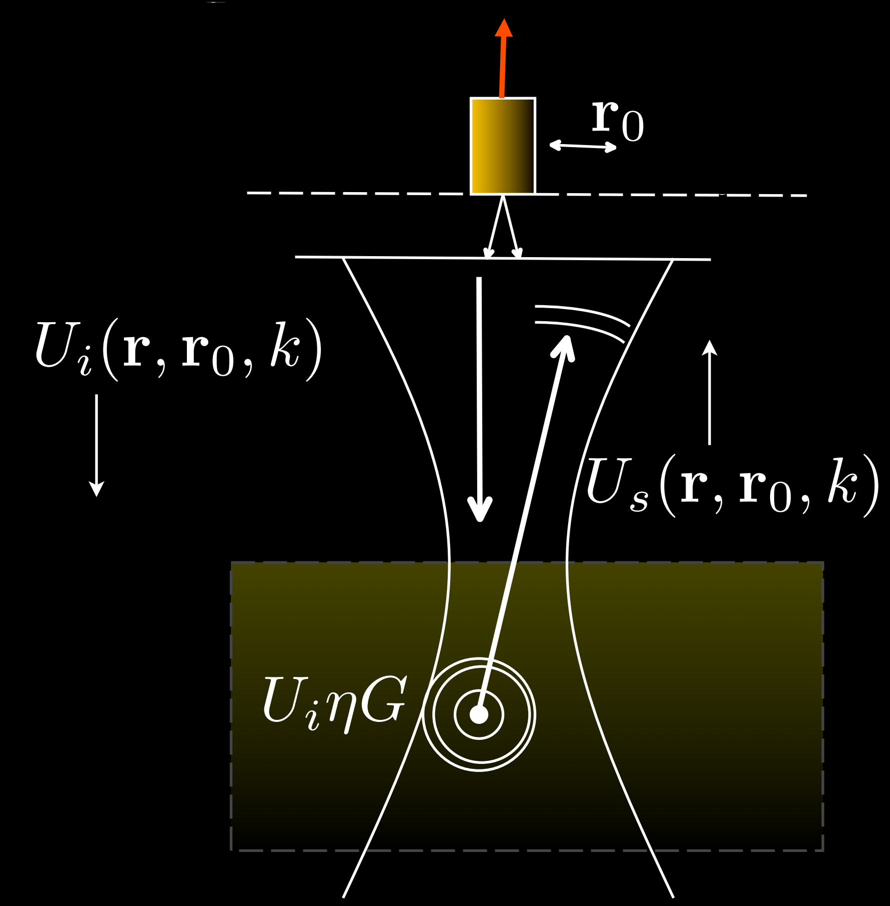

ECE Illinois

Mathematics

$$U_i(\mathbf{r}, \mathbf{r}_0, k) = A(k) g(\mathbf{r} - \mathbf{r}_0)$$

$$U_s(\mathbf{r}, \mathbf{r}_0, k) = \int d^3 r' \, G(\mathbf{r}', \mathbf{r}, k) \eta(\mathbf{r}') U_i(\mathbf{r}', \mathbf{r}_0, k)$$

$$S(\mathbf{r}_0, k) = \int_{z=0} d^2 r \, U(\mathbf{r}, \mathbf{r}_0, k) g(\mathbf{r} - \mathbf{r}_0, k)$$

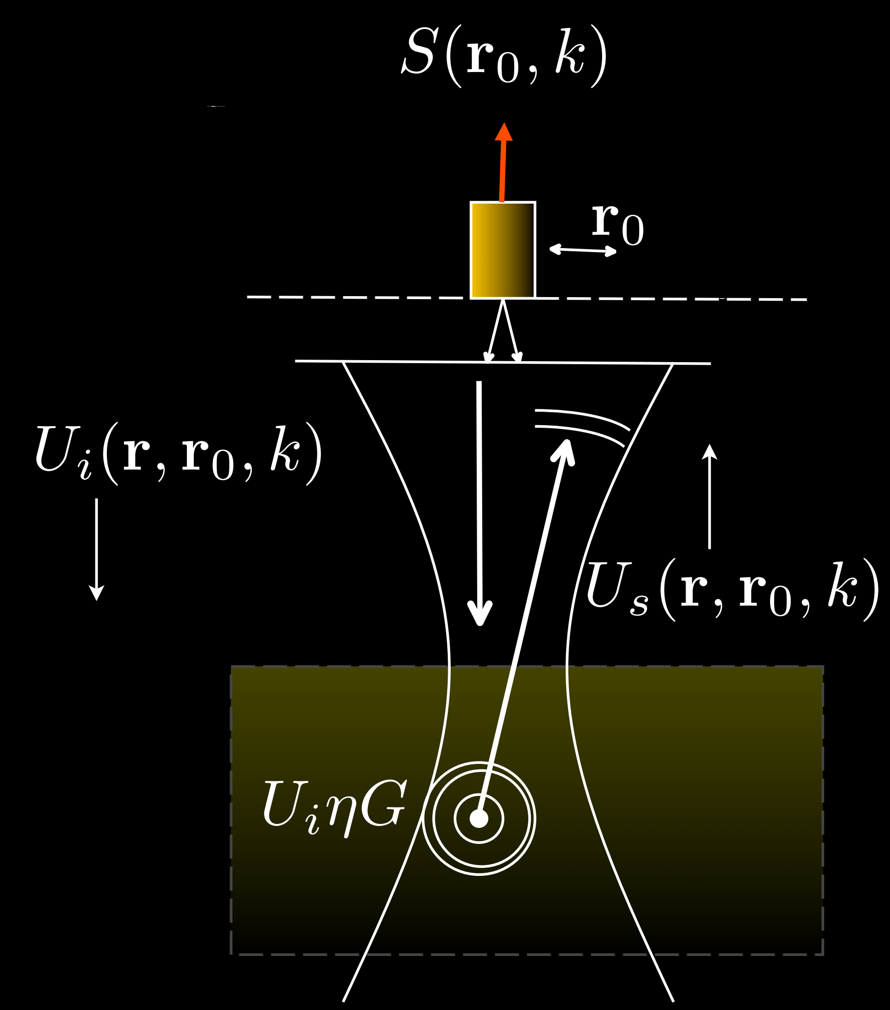

Mathematics

$$U_i(\mathbf{r},\mathbf{r}_0,k) = A(k)g(\mathbf{r}-\mathbf{r}_0)$$

$$U_s(\mathbf{r},\mathbf{r}_0,k) = \int d^3r'\, G(\mathbf{r}',\mathbf{r},k)\eta(\mathbf{r}')U_i(\mathbf{r}',\mathbf{r}_0,k)$$

$$S(\mathbf{r}_0,k) = \int_{z=0} d^2r\, U(\mathbf{r},\mathbf{r}_0,k)g(\mathbf{r}-\mathbf{r}_0,k)$$

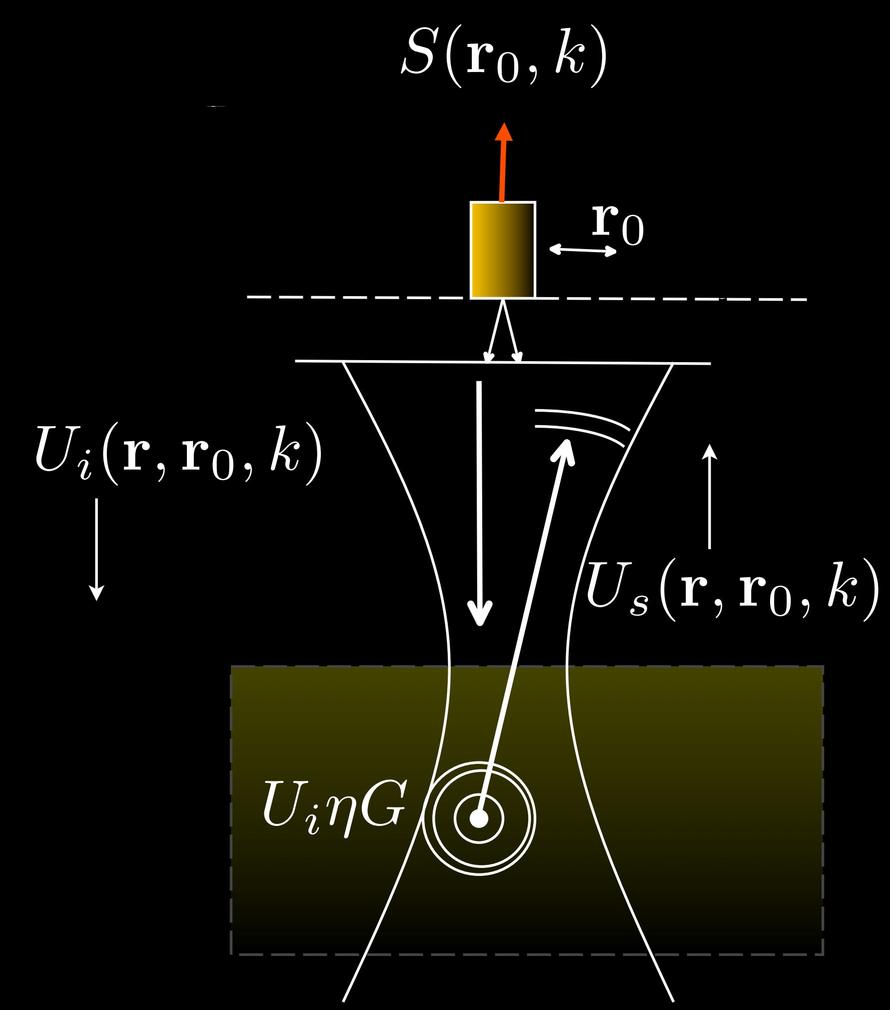

$$S(\mathbf{r}_0,k) = A(k)\int_{z=0} d^2r \int d^3r' G(\mathbf{r}',\mathbf{r},k)g(\mathbf{r}'-\mathbf{r}_0,k)g(\mathbf{r}-\mathbf{r}_0,k)\eta(\mathbf{r}').$$

More math

$$g(\mathbf{r},k) = \frac{1}{2\pi W_0^2(k)} e^{-r^2/2W_0^2(k)}$$

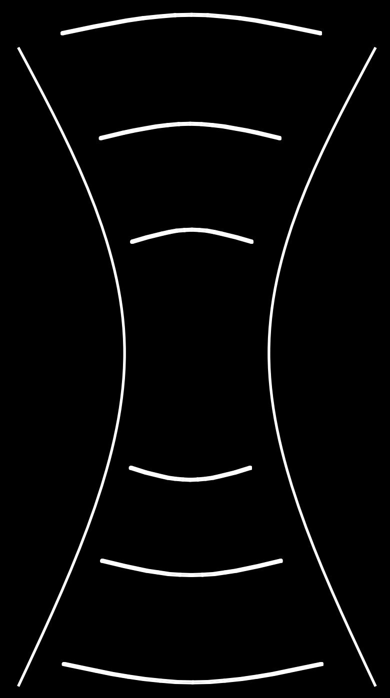

$$\alpha = \pi/NA \qquad W_0(k) = \alpha/k$$

$$\tilde{g}(\mathbf{q},k) = e^{-q^2 W_0^2/2} = e^{-q^2\alpha^2/(2k^2)}$$

$$G(\mathbf{r}',\mathbf{r},k) = \frac{e^{ik|\mathbf{r}-\mathbf{r}'|}}{|\mathbf{r}-\mathbf{r}'|} = \frac{i}{2\pi}\int d^2q\; e^{i\mathbf{q}\cdot(\mathbf{r}-\mathbf{r}')} \frac{e^{-ik_z(\mathbf{q})(z-z')}}{k_z(\mathbf{q})}$$

$$k_z(\mathbf{q}) = \sqrt{k^2 - q^2}$$

Forward simulation

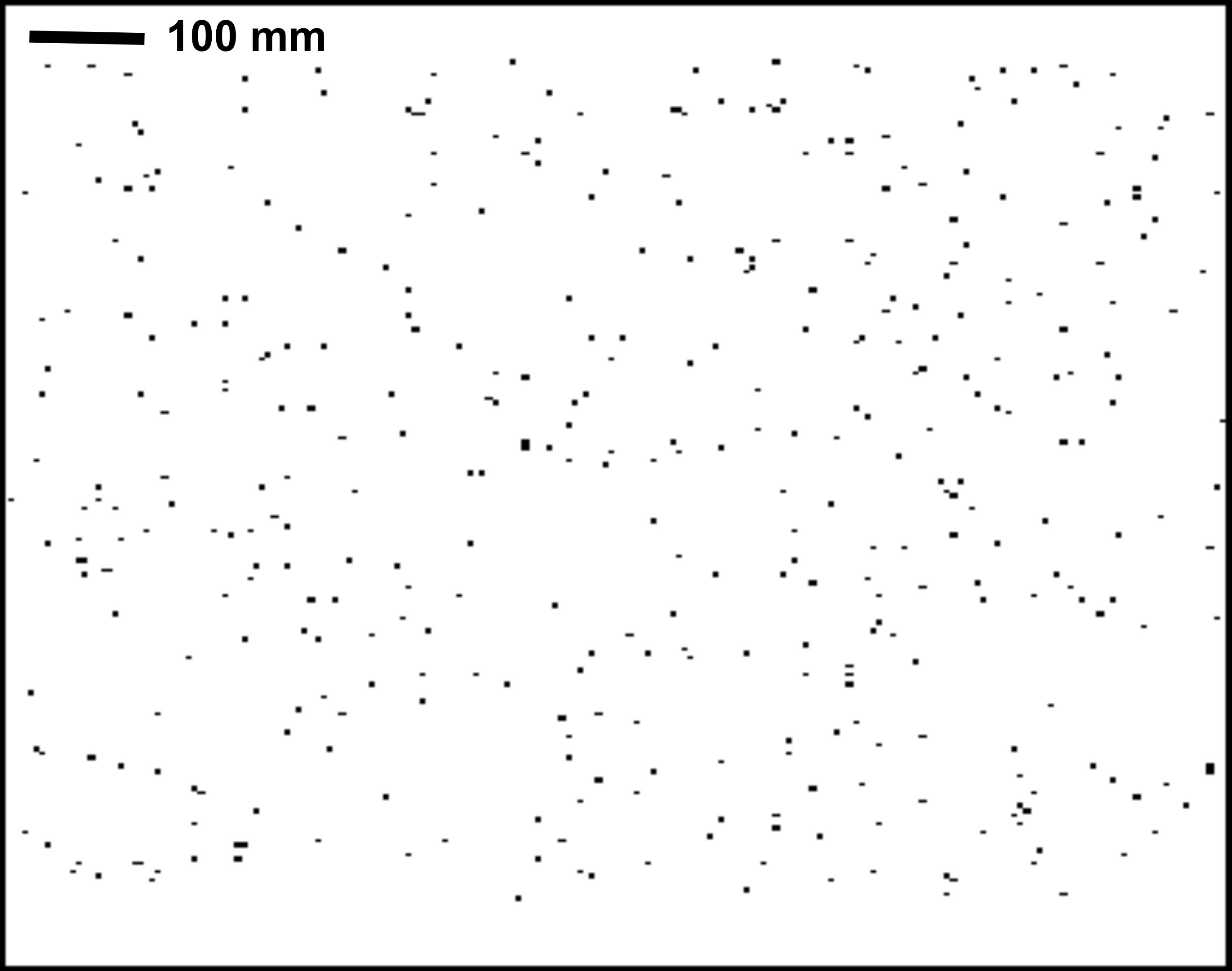

T.S. Ralston, D.L. Marks, F. Kamalabadi, S.A. Boppart. "Deconvolution methods for mitigation of transverse blurring in optical coherence tomography." IEEE Trans. Image Proc. Special Issue on Molecular and Cellular Bioimaging, vol.14, no. 9, September 2005.

T.S. Ralston, D.L. Marks, P.S. Carney, S.A. Boppart, "Inverse scattering for optical coherence tomography," JOSA A, in press.

Forward simulation

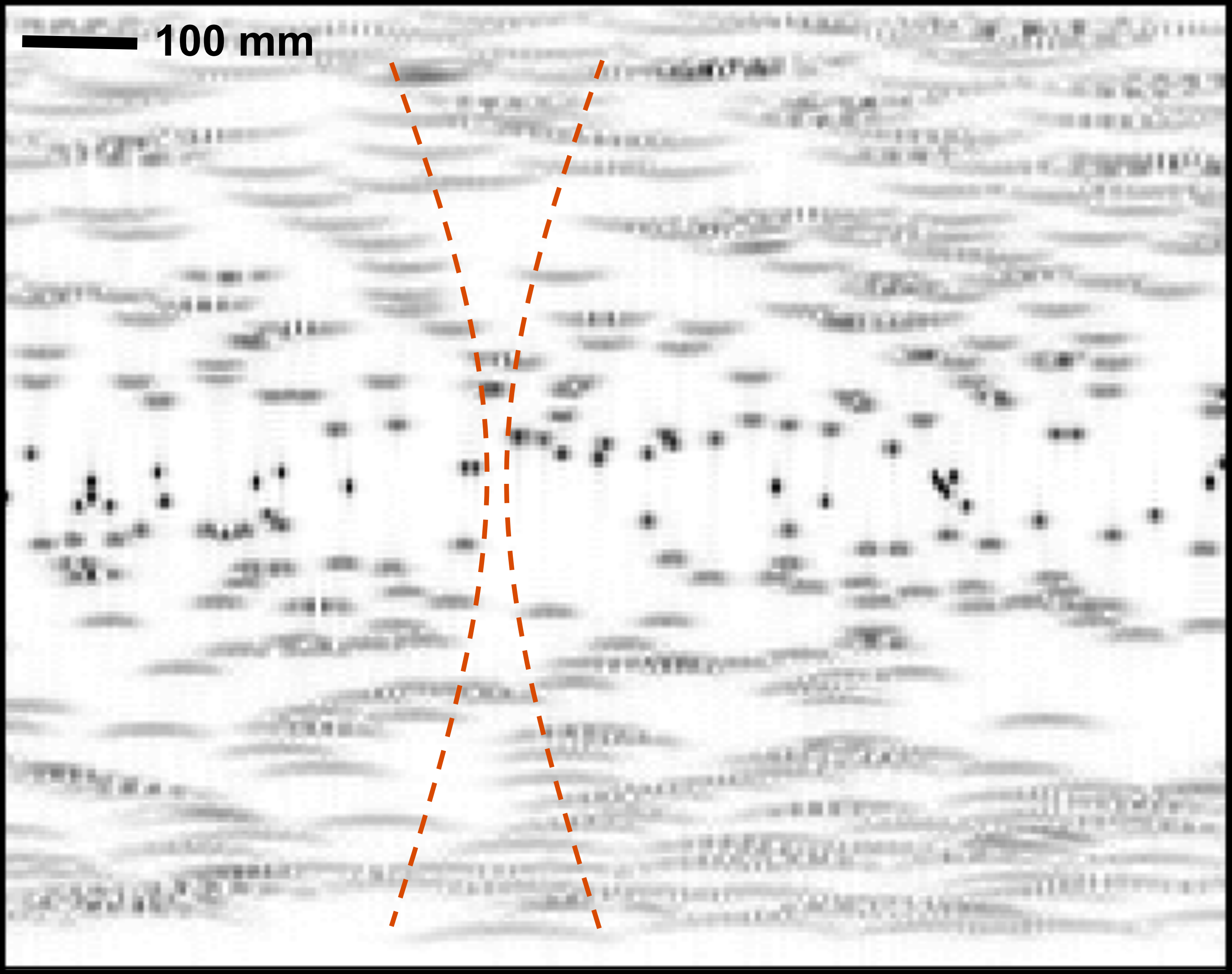

T.S. Ralston, D.L. Marks, F. Kamalabadi, S.A. Boppart. “Deconvolution methods for mitigation of transverse blurring in optical coherence tomography.” IEEE Trans. Image Proc. Special Issue on Molecular and Cellular Bioimaging, vol.14, no. 9, September 2005.

T.S. Ralston, D.L. Marks, P.S. Carney, S.A. Boppart, “Inverse scattering for optical coherence tomography,” JOSA A, in press.

Forward simulation

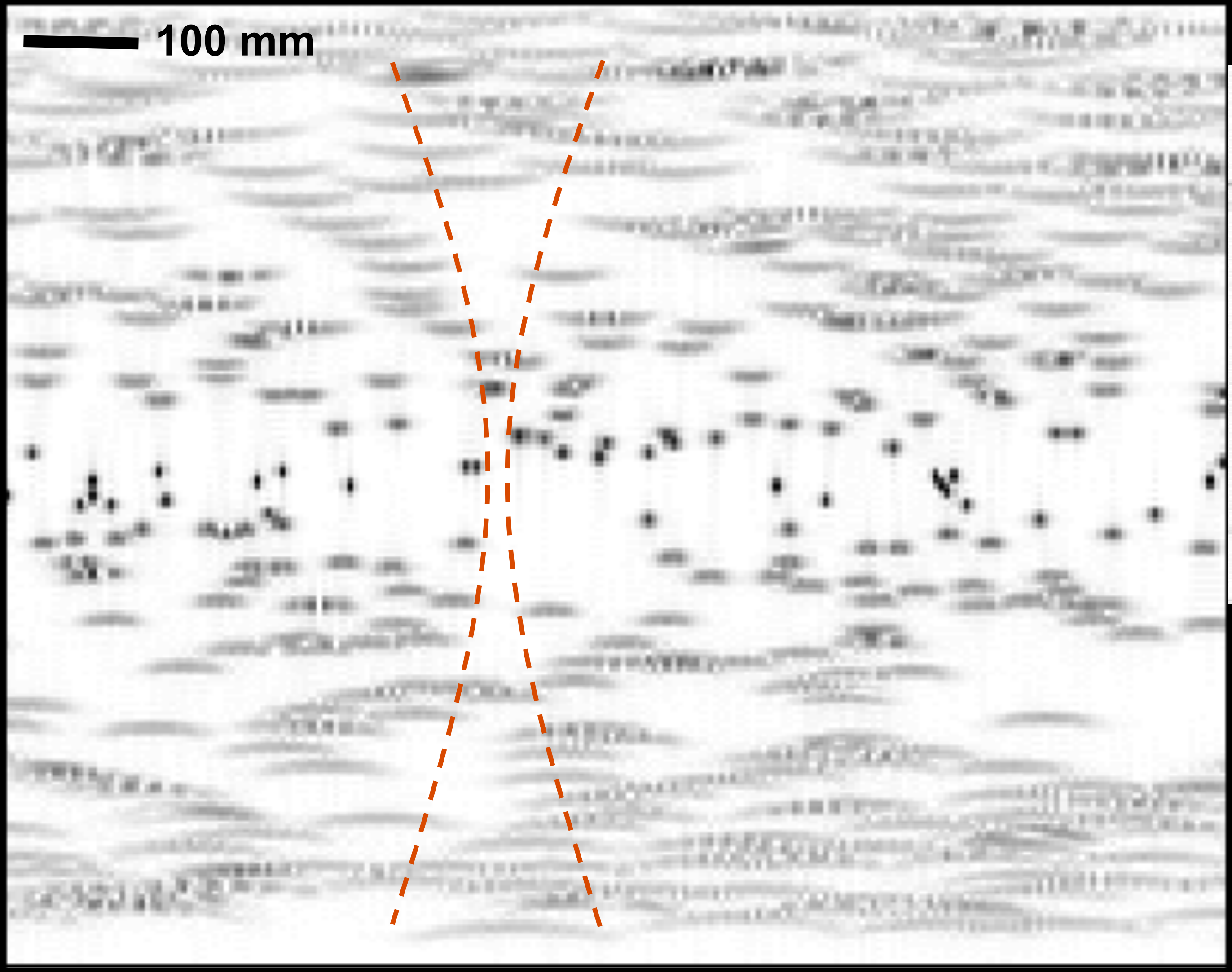

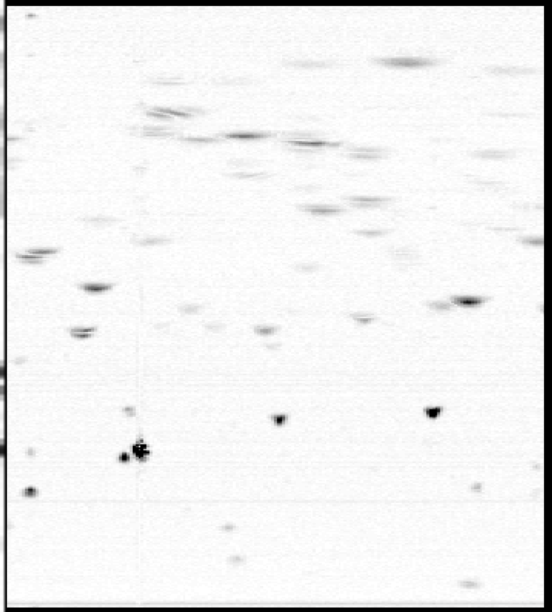

T.S. Ralston, D.L. Marks, F. Kamalabadi, S.A. Boppart. "Deconvolution methods for mitigation of transverse blurring in optical coherence tomography." IEEE Trans. Image Proc. Special Issue on Molecular and Cellular Bioimaging, vol.14, no. 9, September 2005.

T.S. Ralston, D.L. Marks, P.S. Carney, S.A. Boppart, "Inverse scattering for optical coherence tomography," JOSA A, in press.

The inverse problem

$$S(\mathbf{r}_0,k) = A(k)\int_{z=0} d^2r \int d^3r' G(\mathbf{r}',\mathbf{r},k) g(\mathbf{r}'-\mathbf{r}_0,k) g(\mathbf{r}-\mathbf{r}_0,k)\eta(\mathbf{r}').$$

The inverse problem

$$S(\mathbf{r}_0, k) = A(k) \int_{z=0} d^2 r \int d^3 r' G(\mathbf{r}', \mathbf{r}, k) g(\mathbf{r}' - \mathbf{r}_0, k) g(\mathbf{r} - \mathbf{r}_0, k) \eta(\mathbf{r}').$$

$$\tilde{S}(\mathbf{Q}, k) = i2\pi A(k) \int d^2 q \int dz' \, \frac{1}{k_z(\mathbf{q})} e^{ik_z(\mathbf{q})(z'-z_0)} \, e^{ik_z(\mathbf{q}-\mathbf{Q})(z'-z_0)}$$

$$\times \, e^{\frac{-\alpha^2 Q^2}{4k^2}} \, e^{\frac{-\alpha^2 |\mathbf{q}-\mathbf{Q}/2|^2}{k^2}} \, \tilde{\eta}(\mathbf{Q}, z')$$

The inverse problem

$$S(\mathbf{r}_0, k) = A(k) \int_{z=0} d^2 r \int d^3 r' G(\mathbf{r}', \mathbf{r}, k) g(\mathbf{r}' - \mathbf{r}_0, k) g(\mathbf{r} - \mathbf{r}_0, k) \eta(\mathbf{r}').$$

$$\tilde{S}(\mathbf{Q}, k) = i2\pi A(k) \int d^2 q \int dz' \frac{1}{k_z(\mathbf{q})} e^{ik_z(\mathbf{q})(z'-z_0)} e^{ik_z(\mathbf{q}-\mathbf{Q})(z'-z_0)}$$

$$\times e^{\frac{-\alpha^2 Q^2}{4k^2}} e^{\frac{-\alpha^2 |\mathbf{q}-\mathbf{Q}/2|^2}{k^2}} \tilde{\eta}(\mathbf{Q}, z')$$

asymptotic expansion

The inverse problem

$$S(\mathbf{r}_0, k) = A(k) \int_{z=0} d^2 r \int d^3 r' G(\mathbf{r}', \mathbf{r}, k) g(\mathbf{r}' - \mathbf{r}_0, k) g(\mathbf{r} - \mathbf{r}_0, k) \eta(\mathbf{r}').$$

$$\tilde{S}(\mathbf{Q}, k) = i2\pi A(k) \int d^2 q \int dz' \, \frac{1}{k_z(\mathbf{q})} e^{ik_z(\mathbf{q})(z'-z_0)} \, e^{ik_z(\mathbf{q}-\mathbf{Q})(z'-z_0)}$$

$$\times \, e^{\frac{-\alpha^2 Q^2}{4k^2}} \, e^{\frac{-\alpha^2 |\mathbf{q}-\mathbf{Q}/2|^2}{k^2}} \, \tilde{\eta}(\mathbf{Q}, z')$$

asymptotic expansion

$$\tilde{S}(\mathbf{Q}, k) = \frac{k^2}{\alpha^2} i2\pi^2 A(k) \frac{e^{-2ik_z(\mathbf{Q}/2)z_0}}{k_z(\mathbf{Q}/2)} \, e^{\frac{-\alpha^2 Q^2}{4k^2}} \, \tilde{\tilde{\eta}}\left[\mathbf{Q}, -2k_z(\mathbf{Q}/2)\right]$$

Solution and regularization

$$\tilde{S}(\mathbf{Q},k) = K(\mathbf{Q},k)\,\tilde{\tilde{\eta}}\left[\mathbf{Q}, -2k_z(\mathbf{Q}/2)\right]$$

Tikhonov solution:

$$\tilde{\tilde{\eta}}(\mathbf{Q},\beta) = \left[\frac{K^*(\mathbf{Q},k,\beta)\tilde{S}(\mathbf{Q},k)}{\left|K(\mathbf{Q},k,\beta)\right|^2 + 2Nk/k_z(\mathbf{Q}/2)}\right]_{k=\frac{1}{2}\sqrt{\beta^2-Q^2}}$$

N is the noise floor

Polar vs. Hyperbolic Resampling

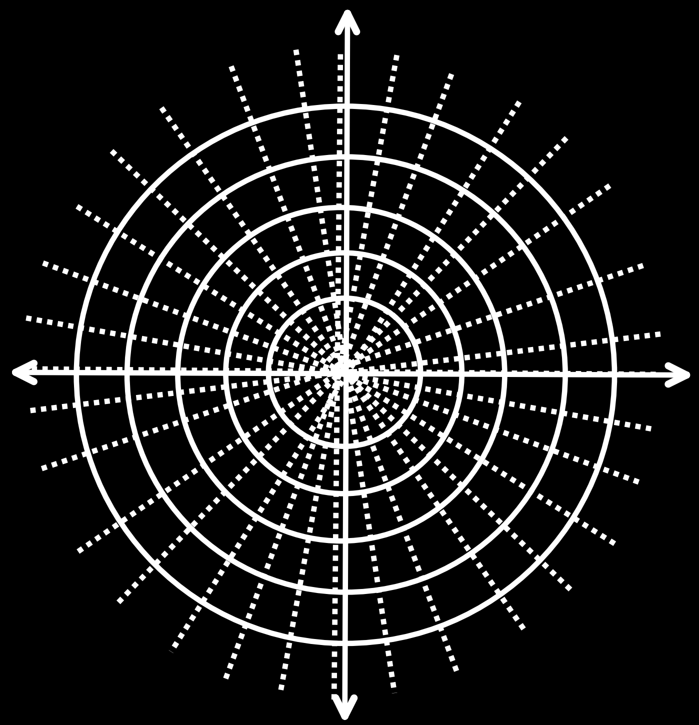

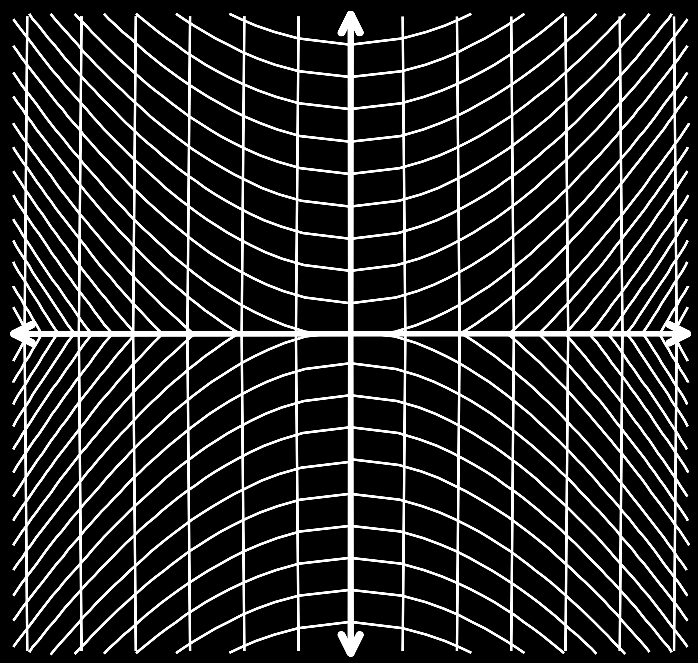

Radon
SAR
MRI
CT

ISAM

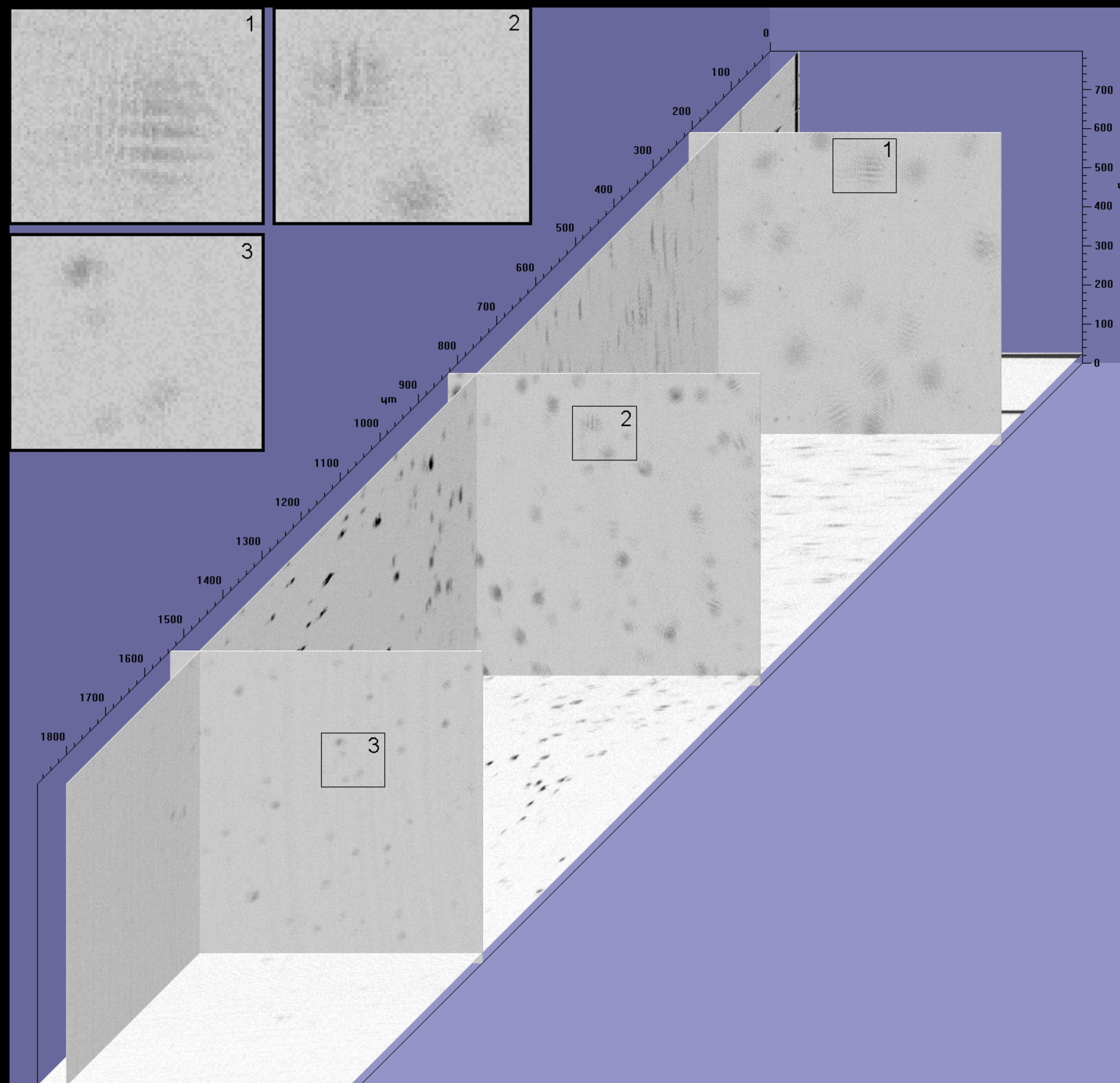
1
2
3
0
100
200
300
400
500
600
700
800
900
μm
1000
1100
1200
1300
1400
1500
1600
1700
1800
0
100
200
300
400
500
600
700
1
2
3

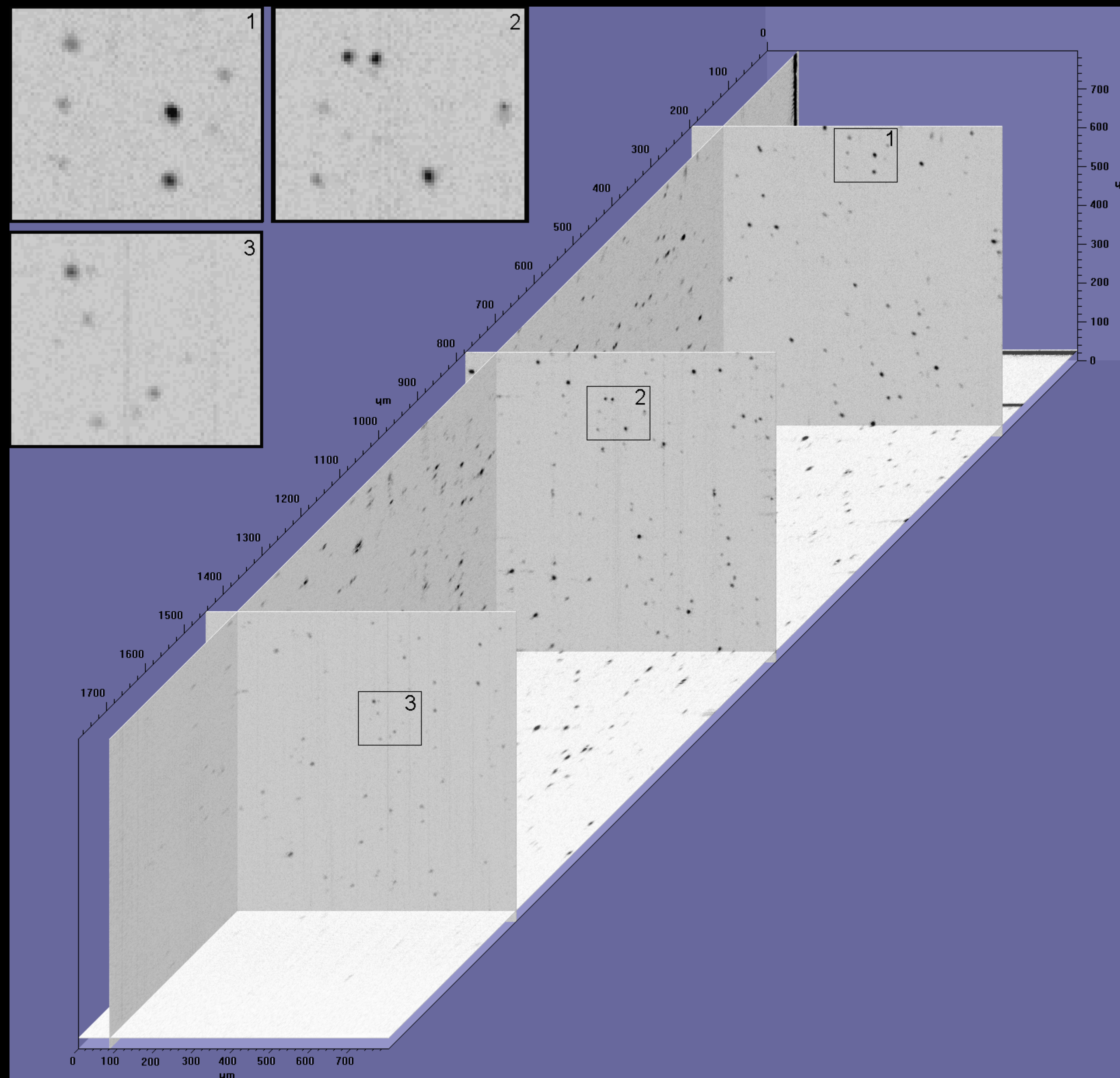
1
2
3
0
100
200
300
400
500
600
700
800
900
μm
1000
1100
1200
1300
1400
1500
1600
1700
0
100
200
300
400
500
600
700
μm
700
600
500
400
300
200
100
0
μm

3D Rendered

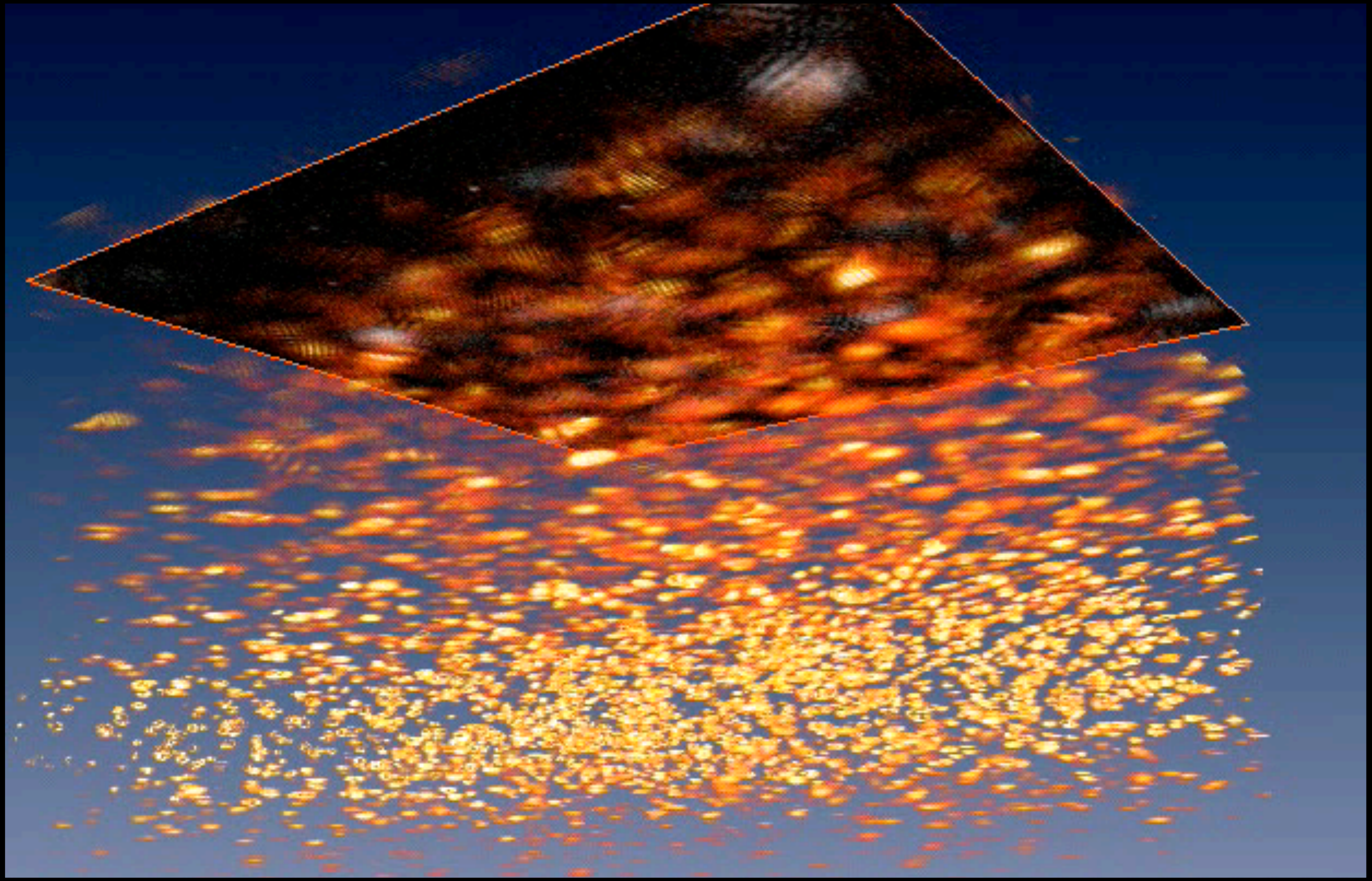

3D Rendered

ECE Illinois

ISAM vs Histology

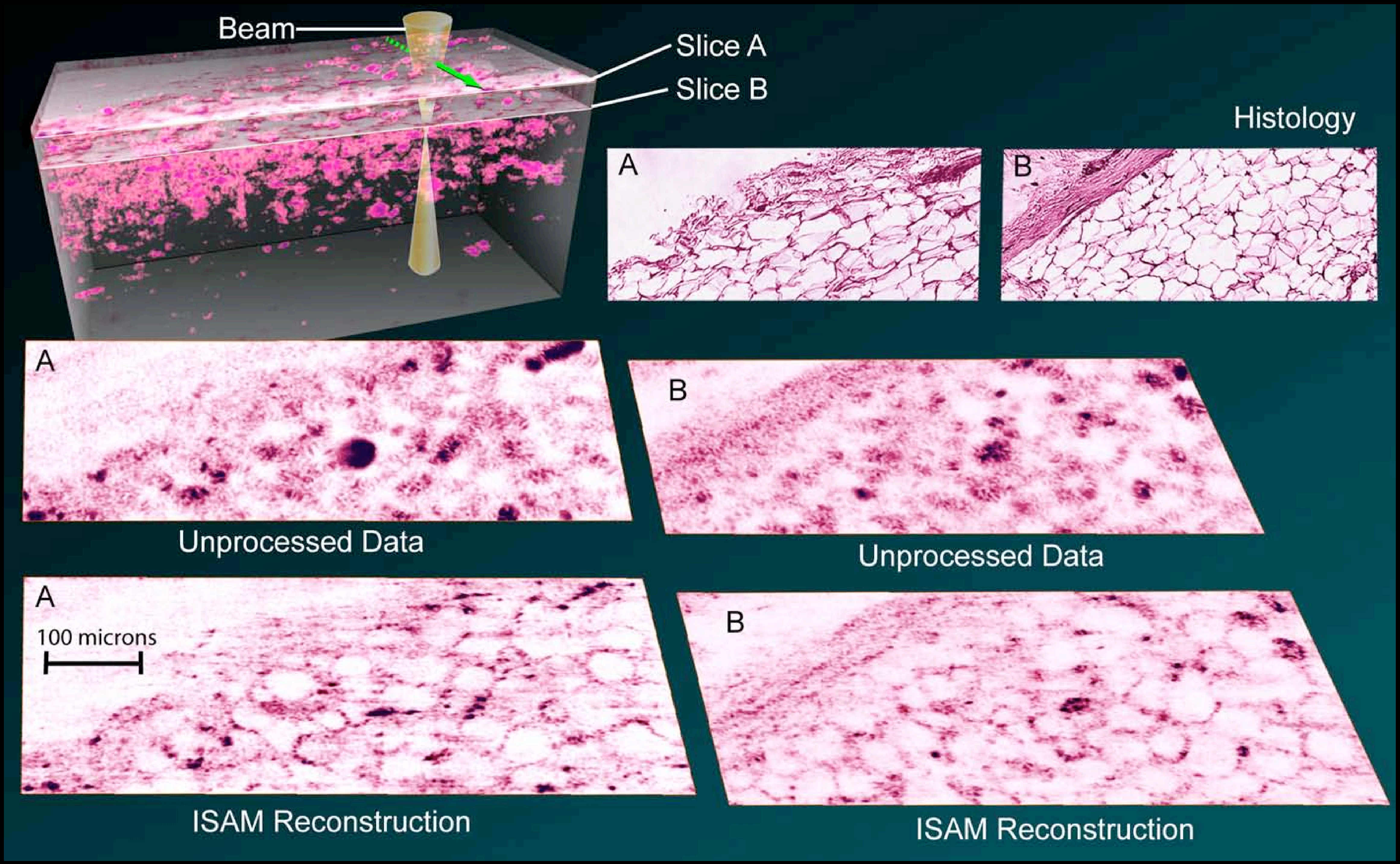

And now for something completely different

- Near-field
- Also scanning
- Also interferometric
- Harder

NSOM images

Fig. 4. Resolution in NSOM as a function of the probe-to-sample separation. The separation in each case is (**A**) near contact; (**B**) 5 nm; (**C**) 10 nm; (**D**) 25 nm; (**E**) 100 nm; and (**F**) 400 nm.

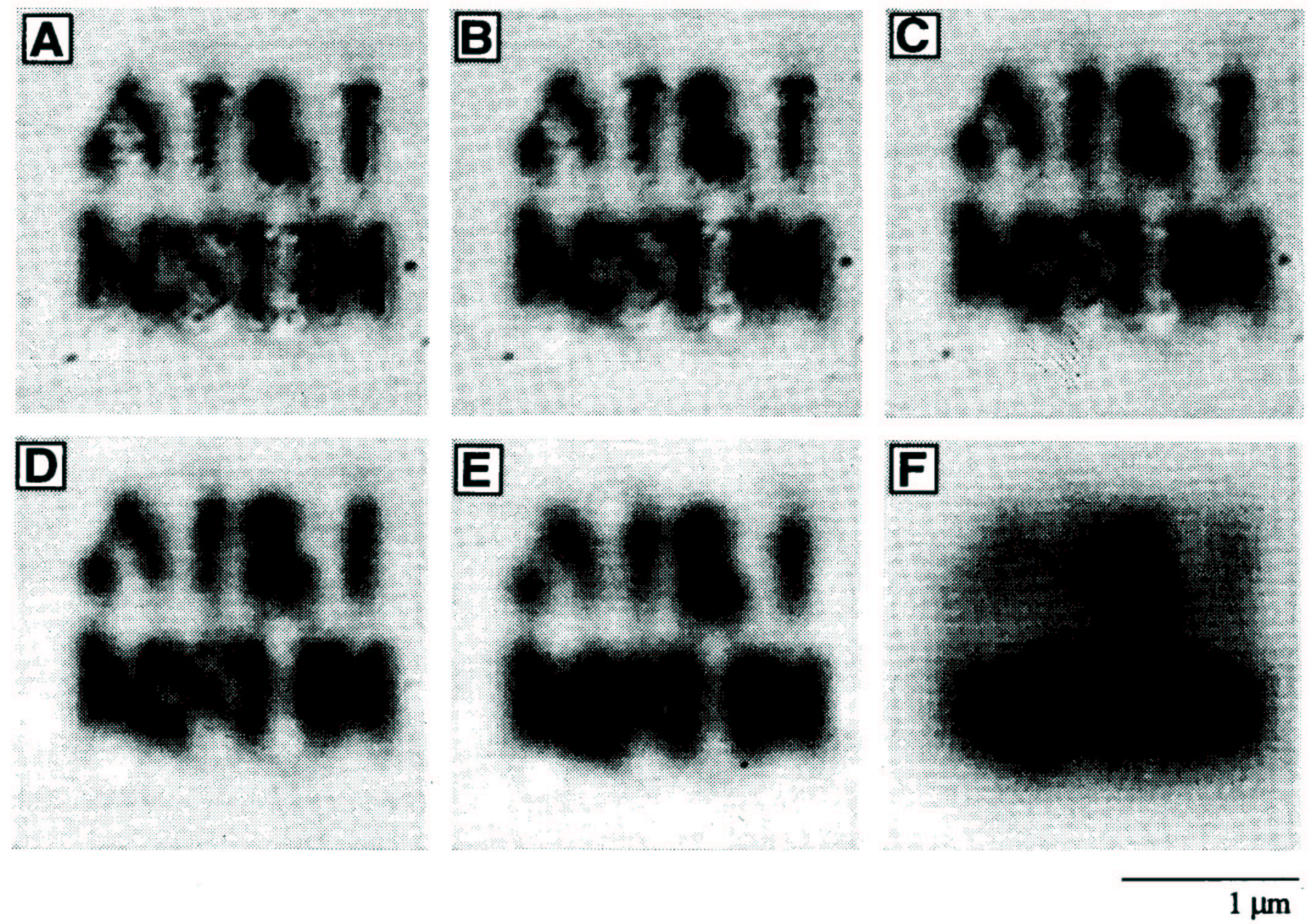

Betzig and Trautman, Science **257**,189-195 (1992).

PSTM holograms

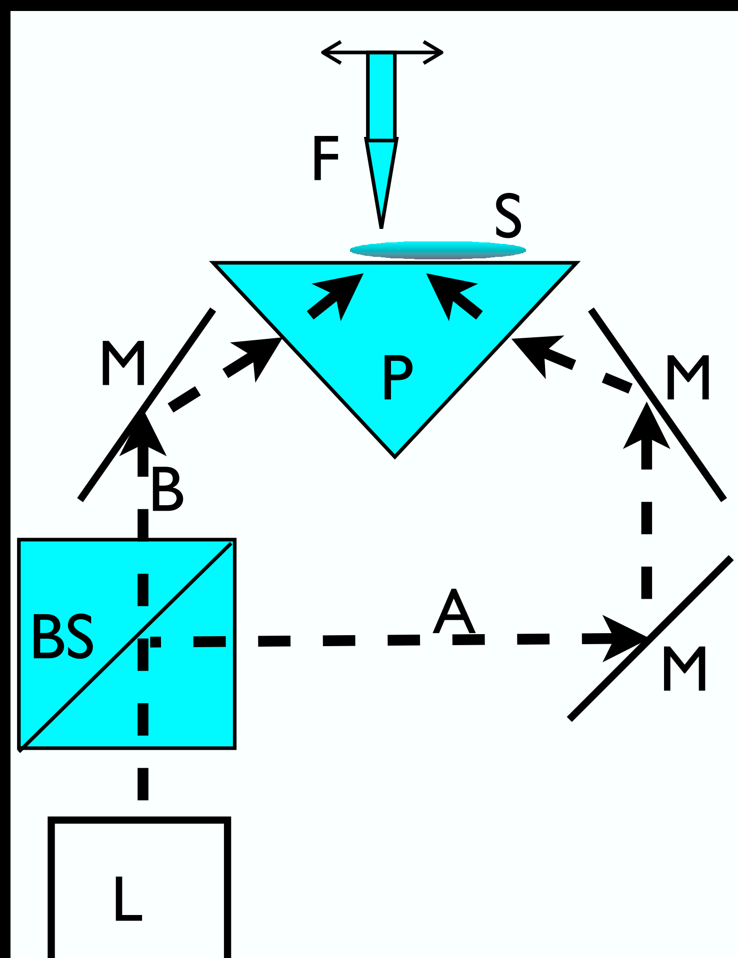

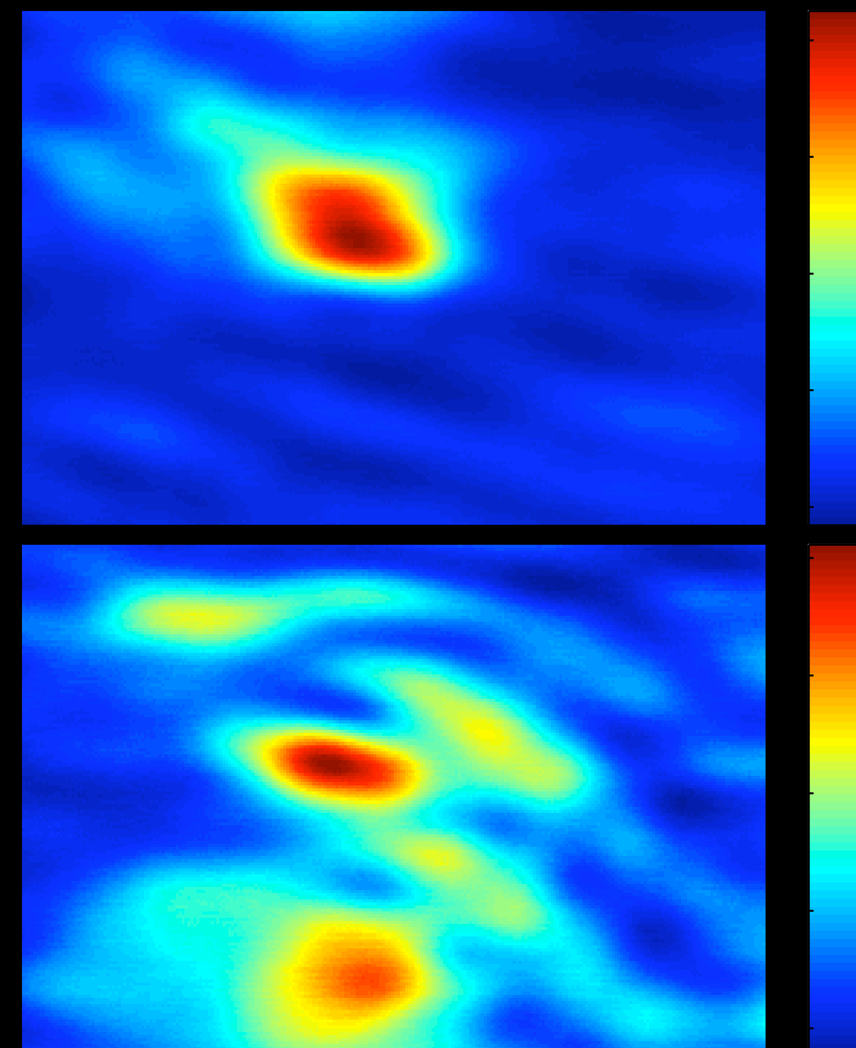

$3\mu m \times 5\mu m$

PSTM/NSOM simple model

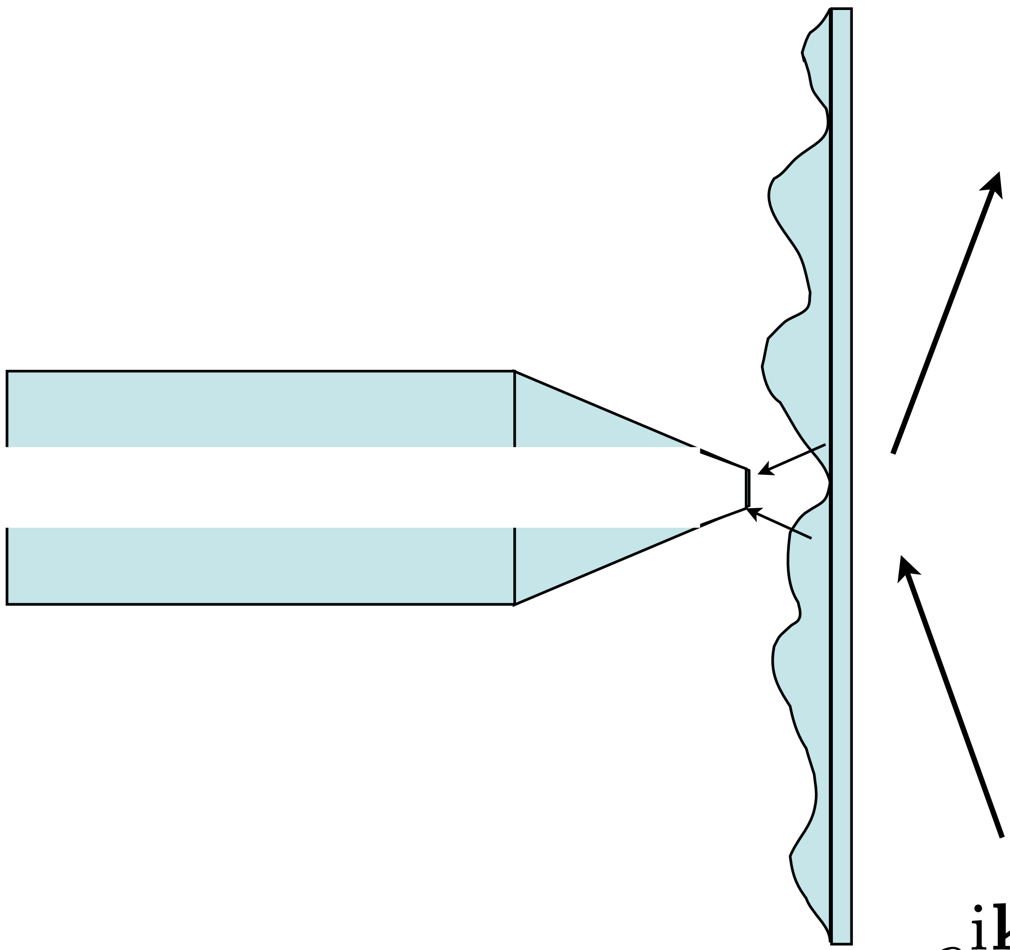

$$e^{\mathrm{i}\mathbf{k}(\mathbf{q})\cdot\mathbf{r}}$$

$$\mathbf{k}(\mathbf{q}) = (\mathbf{q}, \sqrt{k_0^2 - q^2})$$

Monochromatic field $\omega_0 = ck_0$

$$U_{\mathbf{q}}(\mathbf{r}) = \int \mathrm{d}^3 r' \; e^{\mathrm{i}\mathbf{k}(\mathbf{q})\cdot\mathbf{r}'} G(\mathbf{r}, \mathbf{r}') V(\mathbf{r}')$$

$$K_{\mathbf{q}}(\mathbf{r}; \mathbf{r}') = \int \mathrm{d}^2 Q \; \lambda_{\mathbf{Q}}^{\mathbf{q}} g_{\mathbf{Q}}^{\mathbf{q}}(r) f_{\mathbf{Q}}^{\mathbf{q}*}(\mathbf{r}')$$

$$g_{\mathbf{Q}}^{\mathbf{q}}(r) = \frac{e^{\mathrm{i}(\mathbf{Q}+\mathbf{q})\cdot\mathbf{r}}}{2\pi}$$

$$f_{\mathbf{Q}}^{\mathbf{q}*}(\mathbf{r}') = \frac{-\mathrm{i}e^{\mathrm{i}\mathbf{Q}\cdot\mathbf{r}' - \mathrm{i}|z'|k_z^*(\mathbf{Q}+\mathbf{q}) - \mathrm{i}zk_z^*(\mathbf{q})}}{4\pi k_z^*(\mathbf{Q}+\mathbf{q})\lambda_{\mathbf{Q}}^{\mathbf{q}}}$$

Calculation of the pseudo-inverse

$$M_{\mathbf{q}\mathbf{q}'}(\mathbf{Q})\delta^{(2)}(\mathbf{Q}-\mathbf{Q}') = \langle f_{\mathbf{Q}}^{\mathbf{q}} | f_{\mathbf{Q}'}^{\mathbf{q}'} \rangle \lambda_{\mathbf{Q}}^{\mathbf{q}} \lambda_{\mathbf{Q}'}^{\mathbf{q}'}$$

$$M(\mathbf{Q})\mathbf{c}_\ell(\mathbf{Q}) = \Lambda_{\mathbf{Q}\ell}\mathbf{c}_\ell(\mathbf{Q})$$

$$\psi_{\mathbf{Q}\ell}(\mathbf{r}') = \Lambda_{\mathbf{Q}\ell}^{-1} \sum_{\mathbf{q}} c_{\ell\mathbf{q}}(\mathbf{Q}) \lambda_{\mathbf{Q}}^{\mathbf{q}} f_{\mathbf{Q}}^{\mathbf{q}}(\mathbf{r}')$$

$$\phi_{\mathbf{Q}\ell\mathbf{q}'}(\mathbf{r}) = c_{\ell\mathbf{q}'}(\mathbf{Q}) g_{\mathbf{Q}}^{\mathbf{q}'}(\mathbf{r})$$

$$K^+(\mathbf{r}'; \mathbf{r}, \mathbf{q}) = \int \mathrm{d}^2 Q \sum_\ell \Lambda_{\mathbf{Q}\ell}^{-1} \psi_{\mathbf{Q}\ell}(\mathbf{r}') \phi_{\mathbf{Q}\ell\mathbf{q}}^*(\mathbf{r})$$

And the results are ...

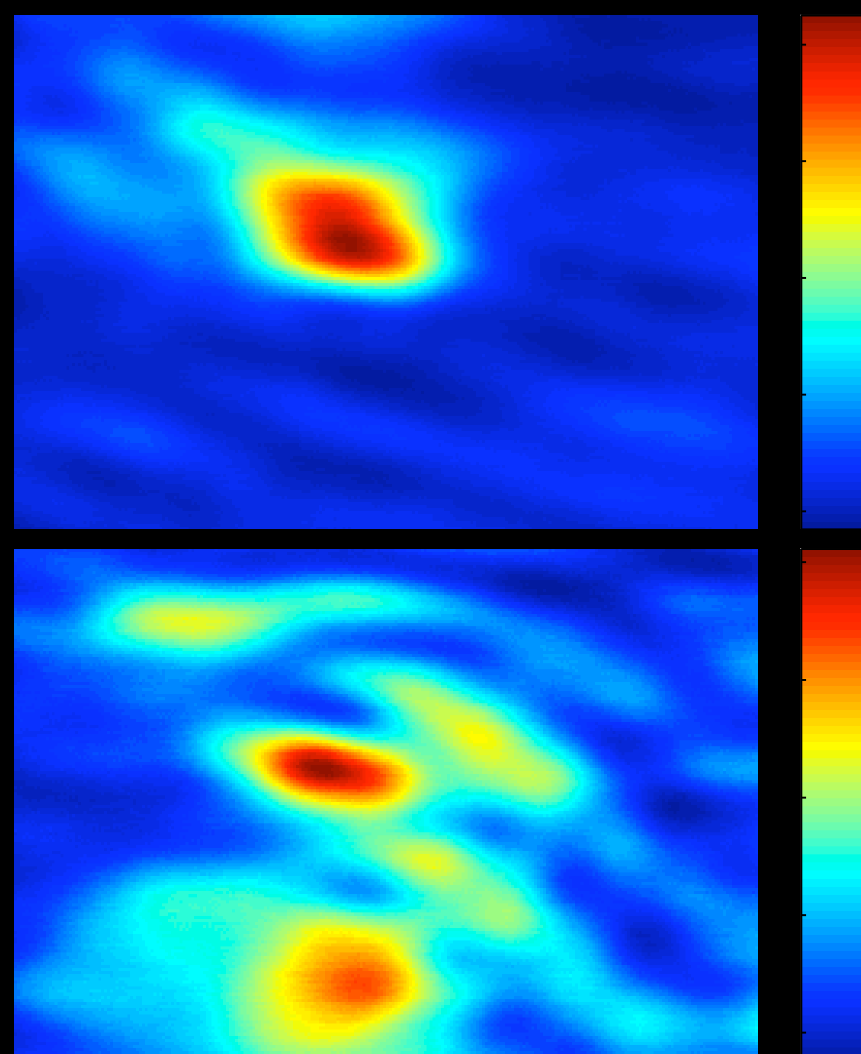

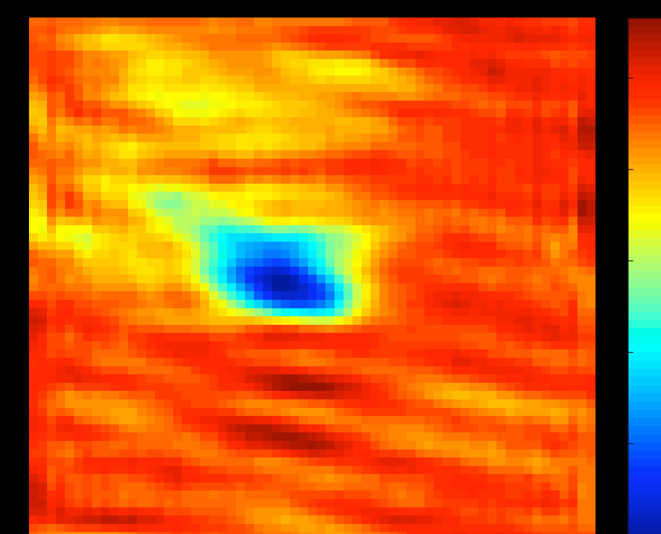

terrible.

Fix the physics: Multiple interactions with the probe

$$U = [TS + ST + TST + TTS + STT + STS + SST + \ldots]U_i$$

collection

resum

illumination

nonlinear

important correction

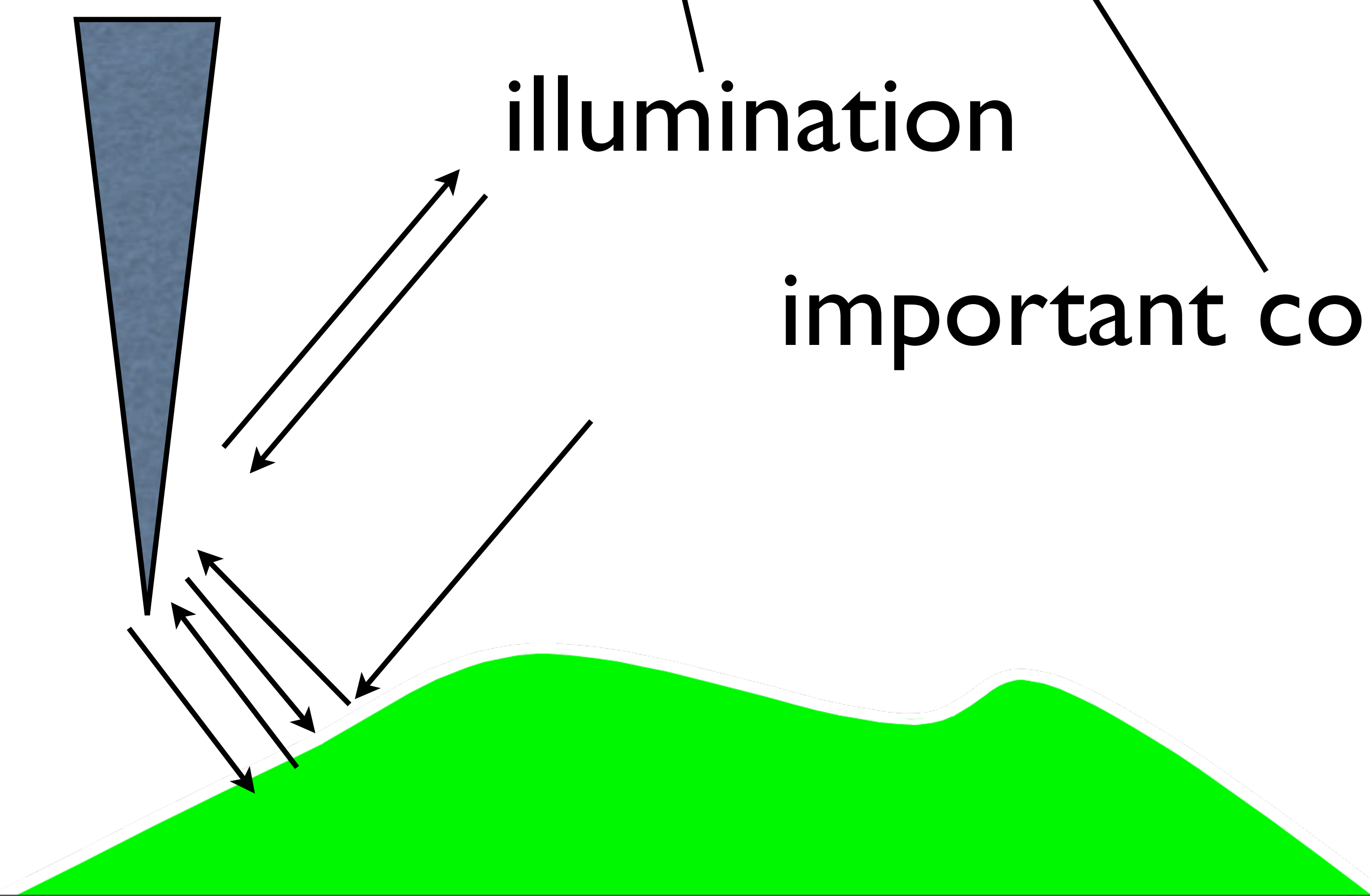

Strong tip corrections

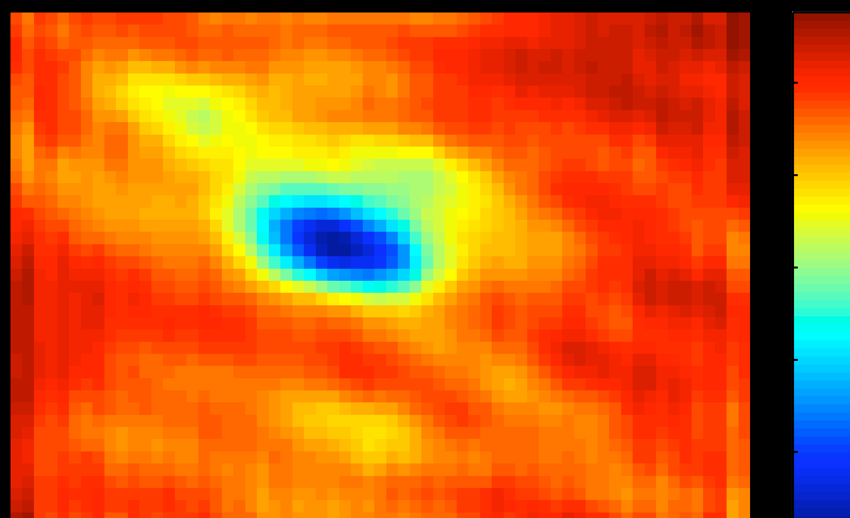

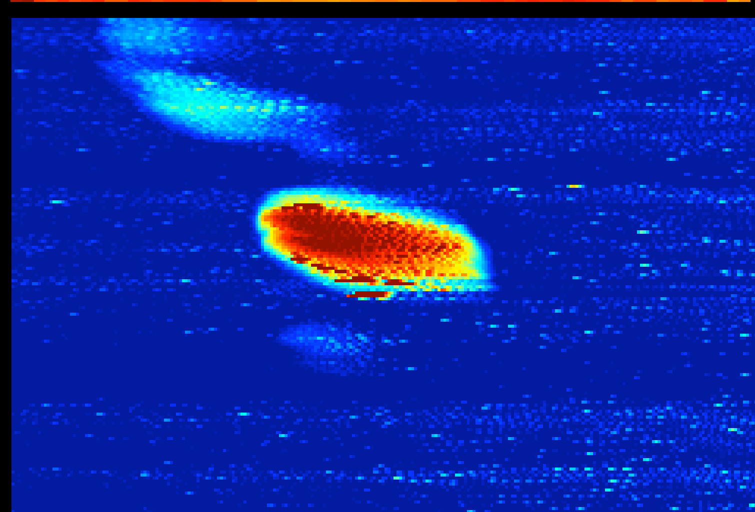

AFM

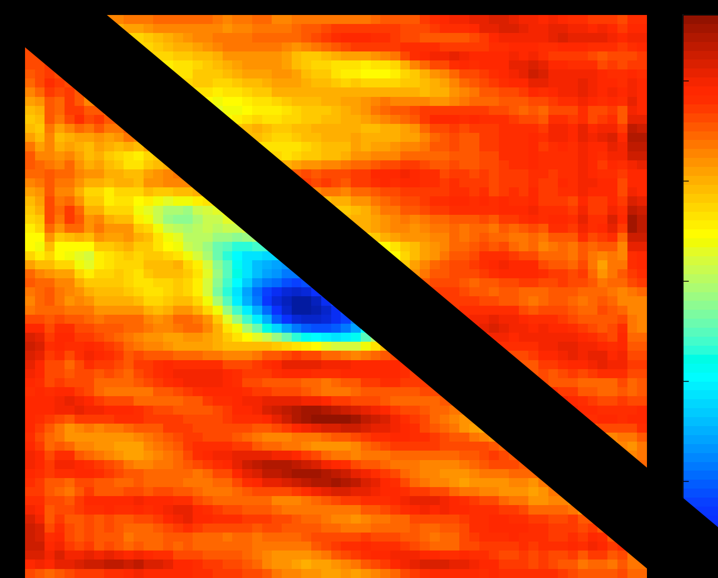

Conclusions

- Inverse scattering and computed imaging extend the utility and scope of data collection methods
- Physics makes it go.
- ISAM is easy and much better that OCT
- NFOT turns holograms into images and 3-d is next.

(End of the standard menu, begin epicurean options)

Cross-validation

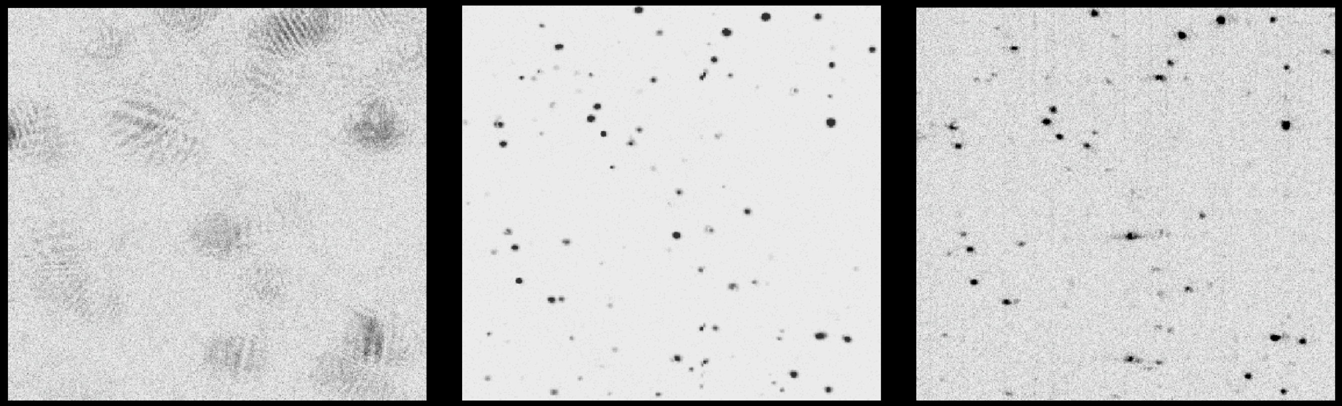

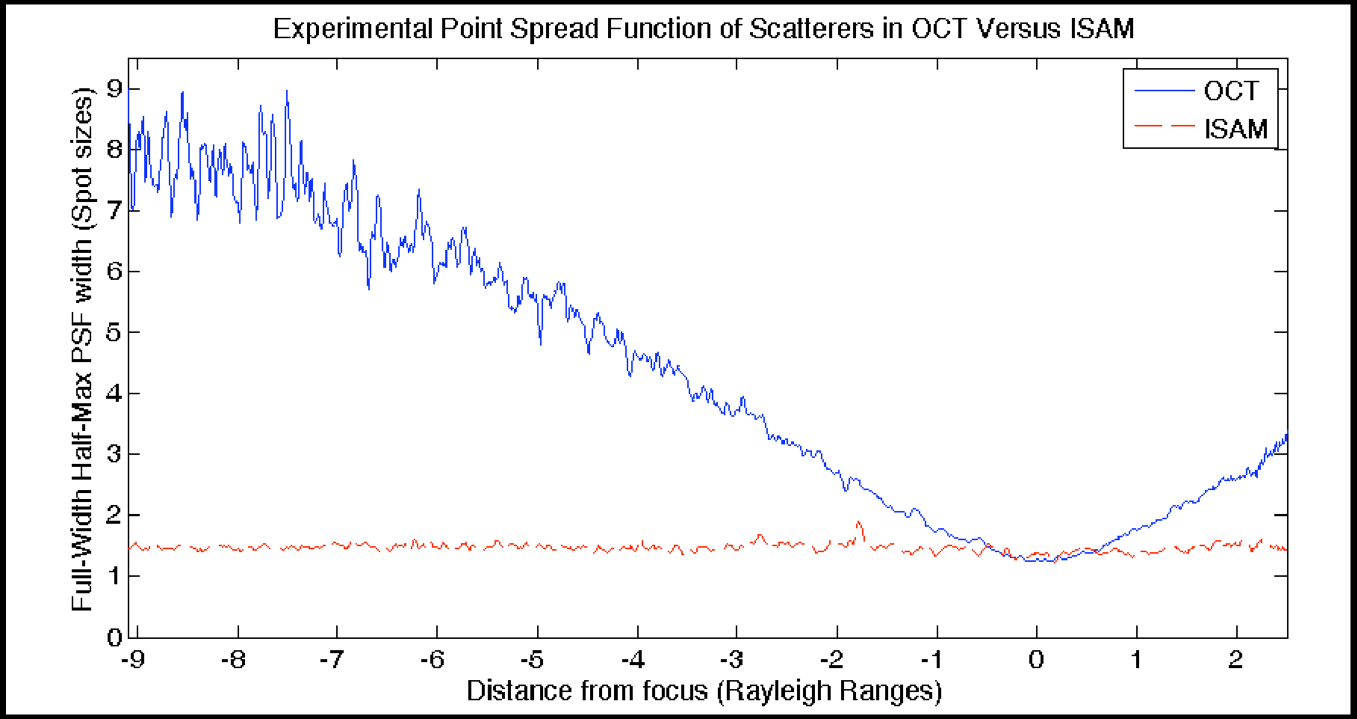

Autocorrelation mitigation

CS LETTERS / Vol. 32, No. 11 / June 1, 2007

d performance in the spectrometer [2].
ter it is assumed that a single measure-
n with τ_0 set such that the real and con-
s can just be separated. A quantitative
he object is made from these data using
d ISAM, and the resulting autocorrela-
are investigated.
$S(\mathbf{r}_\parallel,k)=S_{sr}(\mathbf{r}_\parallel,kc/n)$ can be defined by
m temporal to spatial spectra according
sion relation $k=n\omega/c$. In samples with
rying background properties, a more
tion can be employed and dispersion
digitally [10,15]. Autocorrelation and
age artifacts arise because S_{sr} is not di-
ble, and S is therefore calculated from

the two-dimensional Fourier transform
d by a tilde) with respect to $\mathbf{r}_\parallel$, the most
I model [11] can be written as

$$,k) = \int \widetilde{L}(\mathbf{Q}_\parallel,k,z)e^{i2k_z z}\widetilde{\eta}(\mathbf{Q}_\parallel,z)\mathrm{d}z, \quad (4)$$

$^2-Q_\parallel^2)^{0.5}$ is the axial component of the
η is the object susceptibility, and $\widetilde{L}$ is de-
the specific instrumentation used. When
ence in the factor $\widetilde{L}$ is neglected and it is
t $k_z=k$ (an extreme form of the paraxial
n), the conventional OCT model is re-
hich the transverse and axial effects are
That is, OCT reconstruction may be

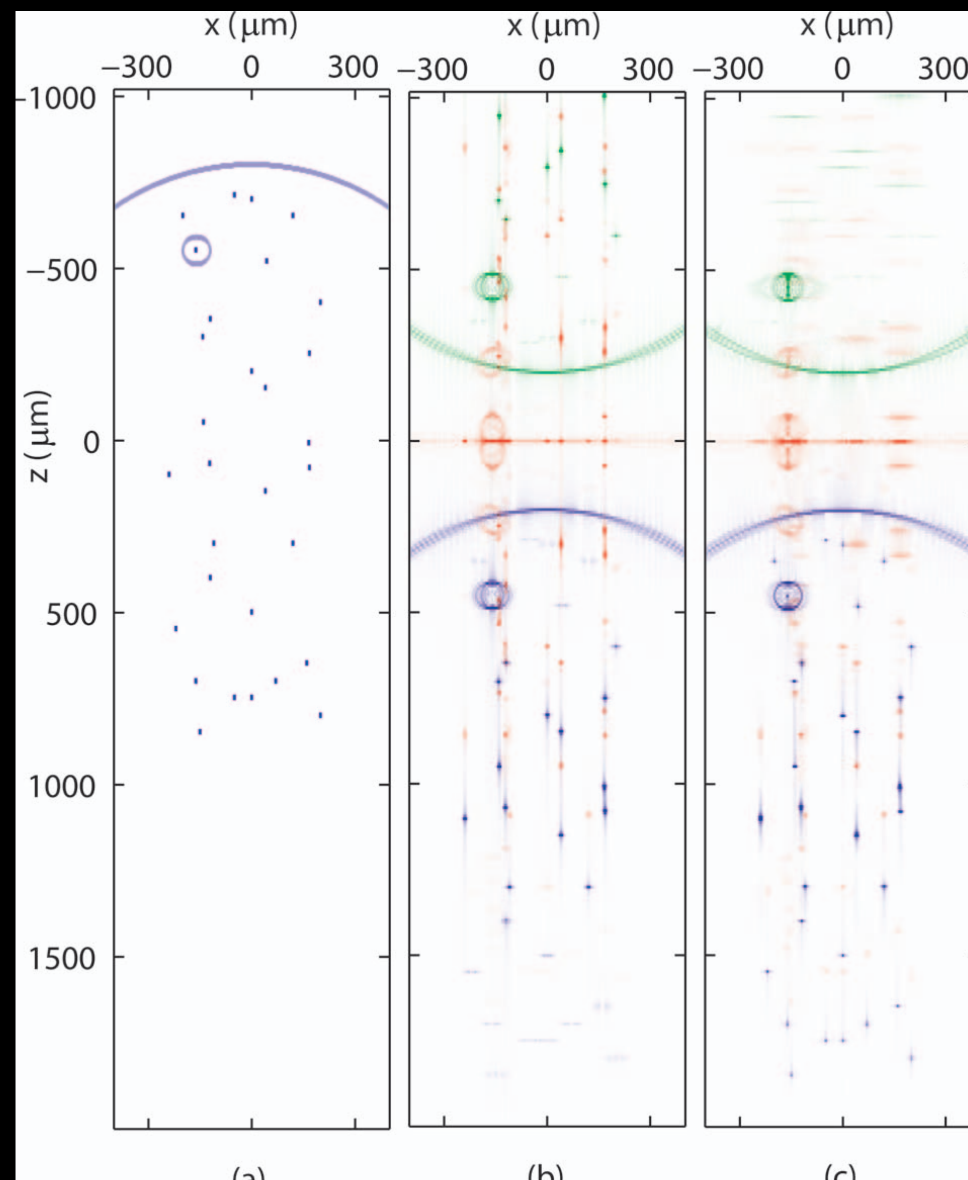

Fig. 1. (a) The $x-z$ plane of the object and (b) the resulting OCT and (c) ISAM images with $c\tau_0=-1$ mm. The structures in (a) have been broadened for display. In (b) and (c) the contribution of R_{sr} is shown in blue, R_{sr}^* (conjugate image) in green, and R_{ss} (autocorrelation) in red. The color scale is clipped at 10% of the maximum signal so that low-level de-

ECE Illinois

Autocorrelation mitigation

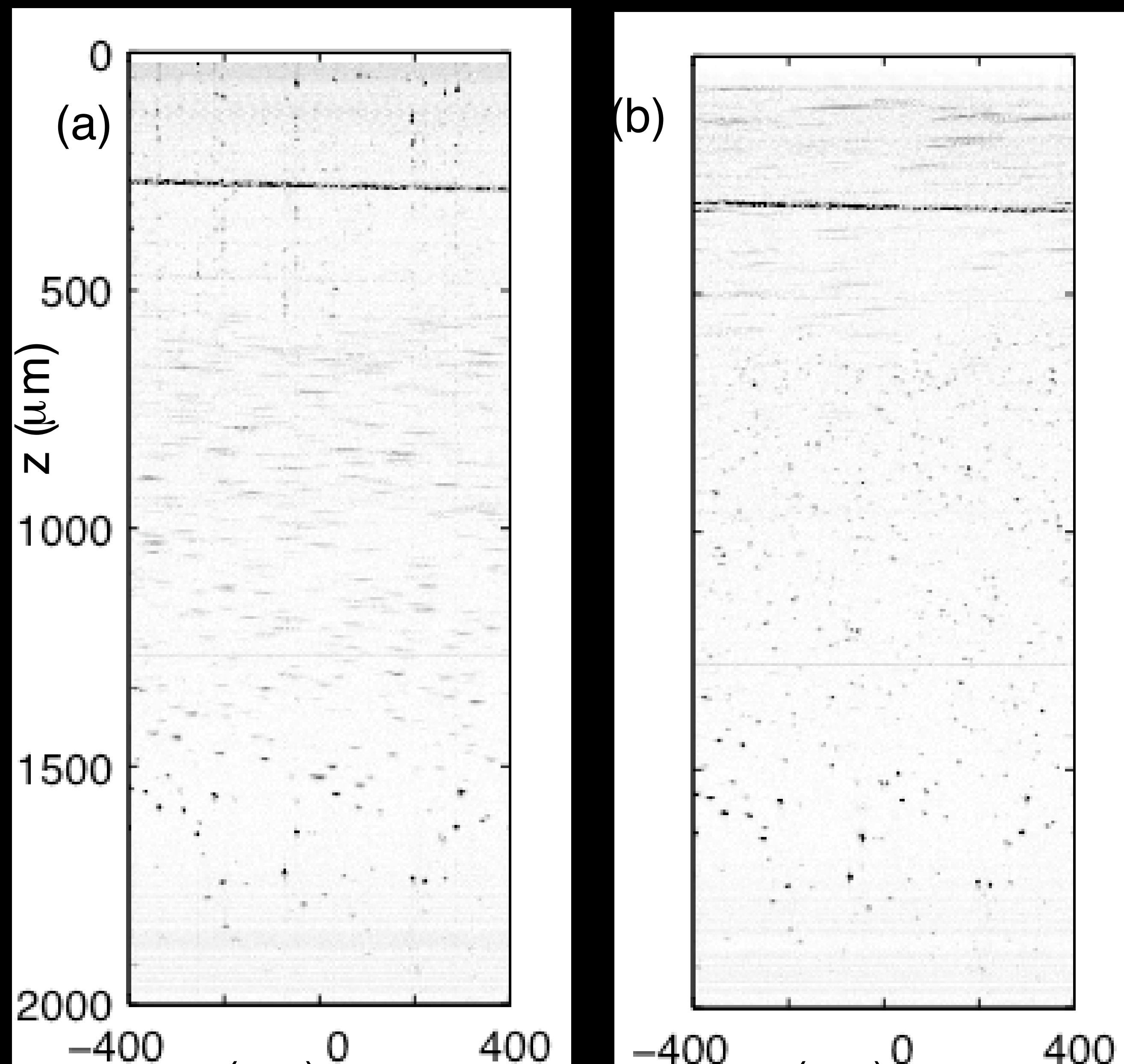

En face Comparison

Unprocessed data **Reconstruction**

Better to be lucky than good

General result for vector fields, high NA:

$$\tilde{S}(\mathbf{Q}_{\|}, k) = \int dz\, \tilde{h}_{\alpha\beta}(\mathbf{Q}_{\|}, z_0 - z; k)\tilde{\eta}_{\alpha\beta}(\mathbf{Q}_{\|}, z)$$

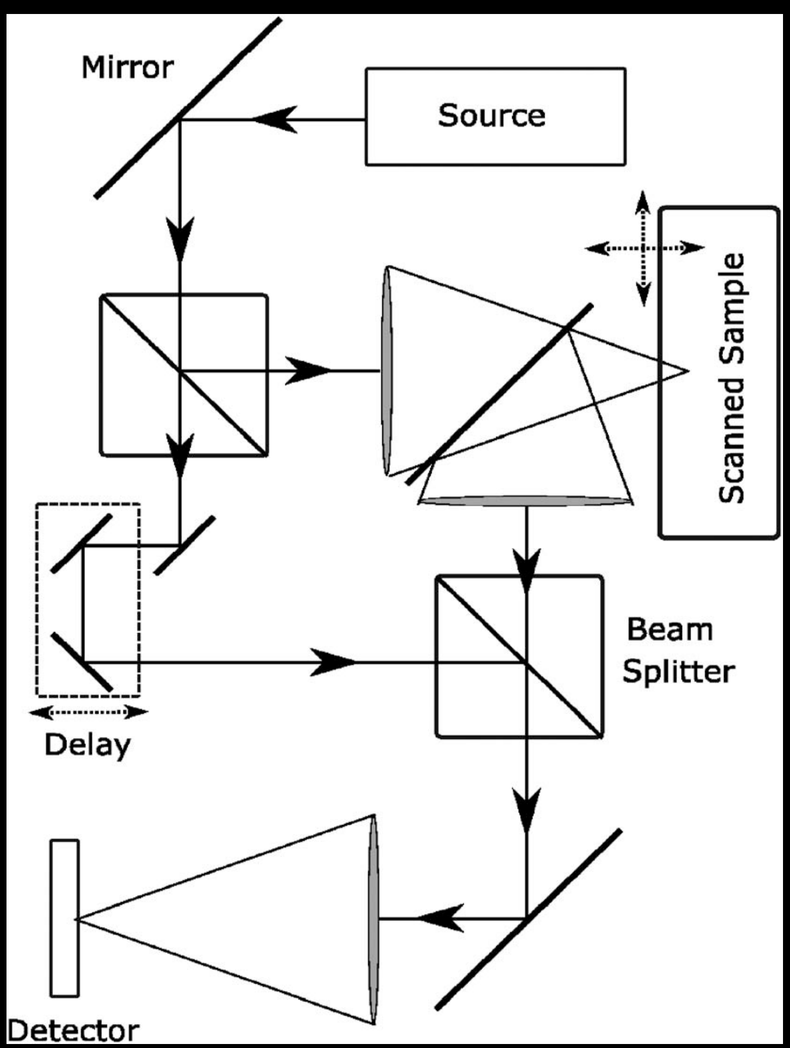

$$\tilde{h}_{\alpha\beta}(-\mathbf{Q}_{\|}, -z; k) =$$

$$-4\pi^2 k\mu_r \left|P(k)\right|^2$$

$$\times \int d^2q_{\|}\ \frac{\hat{F}_\alpha\left(\frac{\mathbf{q}_{\|}}{k}\right)}{\sqrt{k_z(\mathbf{q}_{\|})}}\ \frac{\hat{G}_\beta\left(\frac{\mathbf{Q}_{\|}-\mathbf{q}_{\|}}{k}\right)}{\sqrt{k_z(\mathbf{Q}_{\|}-\mathbf{q}_{\|})}}$$

$$\times e^{i\left[k_z(\mathbf{q}_{\|})+k_z(\mathbf{Q}_{\|}-\mathbf{q}_{\|})\right]z}$$

Battle of the asymptotics

Stationary phase (far from focus)

$$\tilde{h}_{\alpha\beta}(-\mathbf{Q}_{\|}, -z; k) \sim$$

$$\frac{i4\pi^3 k}{z}\mu_r \left|P(k)\right|^2 \ e^{i2k_z(\mathbf{Q}_{\|}/2)z}\hat{F}_\alpha\left(\frac{\mathbf{Q}_{\|}}{2k}\right)\hat{G}_\beta\left(\frac{\mathbf{Q}_{\|}}{2k}\right)$$

Peaked aperture functions (near focus)

$$\tilde{h}_{\alpha\beta}(-\mathbf{Q}_{\|}, -z; k) \sim$$

$$-4\pi^2 k\mu_r \left|P(k)\right|^2 \frac{e^{i\left[k_z(\bar{\mathbf{q}}_{\|})+k_z(\mathbf{Q}_{\|}-\bar{\mathbf{q}}_{\|})\right]z}}{\sqrt{k_z(\bar{\mathbf{q}}_{\|})k_z(\mathbf{Q}_{\|}-\bar{\mathbf{q}}_{\|})}} \int d^2q_{\|}\ \hat{F}_\alpha\left(\frac{\mathbf{q}_{\|}}{k}\right)\hat{G}_\beta\left(\frac{\mathbf{Q}_{\|}-\mathbf{q}_{\|}}{k}\right)$$

EG.

$$\bar{\mathbf{q}}_{\|} = \frac{\mathbf{Q}_{\|}\varsigma_F^2}{\varsigma_F^2 + \varsigma_G^2}$$

Connection to SAR

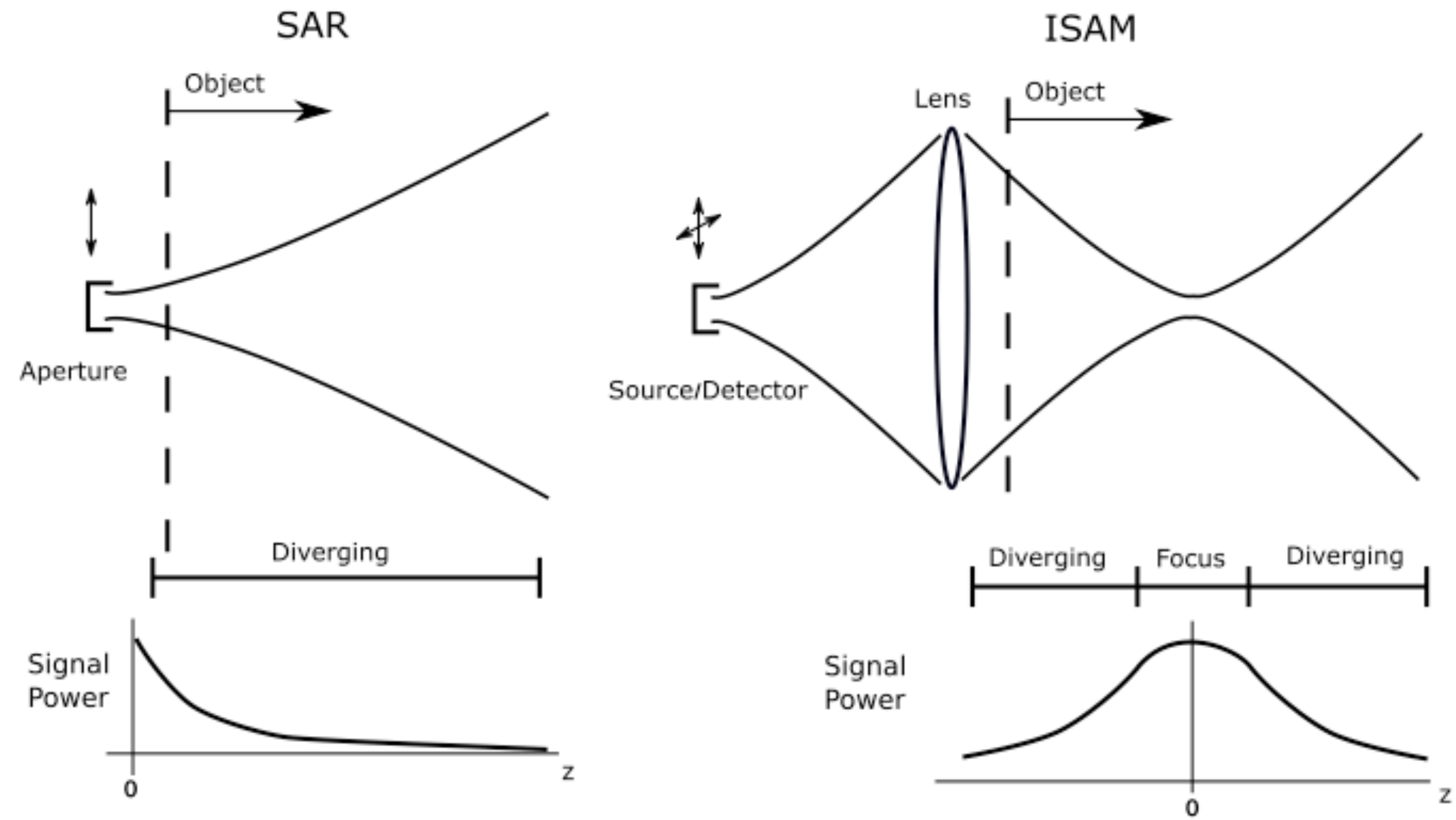

Figure 3. An illustration of the differences between the data acquisition geometries in SAR and ISAM. SAR involves a one-dimensional scan track, while ISAM scans over a plane. Unlike SAR beams, ISAM fields include a region within the object that is in focus. Note that the same aperture is assumed for both transmission and reflection in SAR; similarly the source is imaged onto the detector by the reference arm in ISAM (see Fig. 1). The spectral bands and scan lengths also vary greatly between SAR and ISAM.

SAR and ISAM

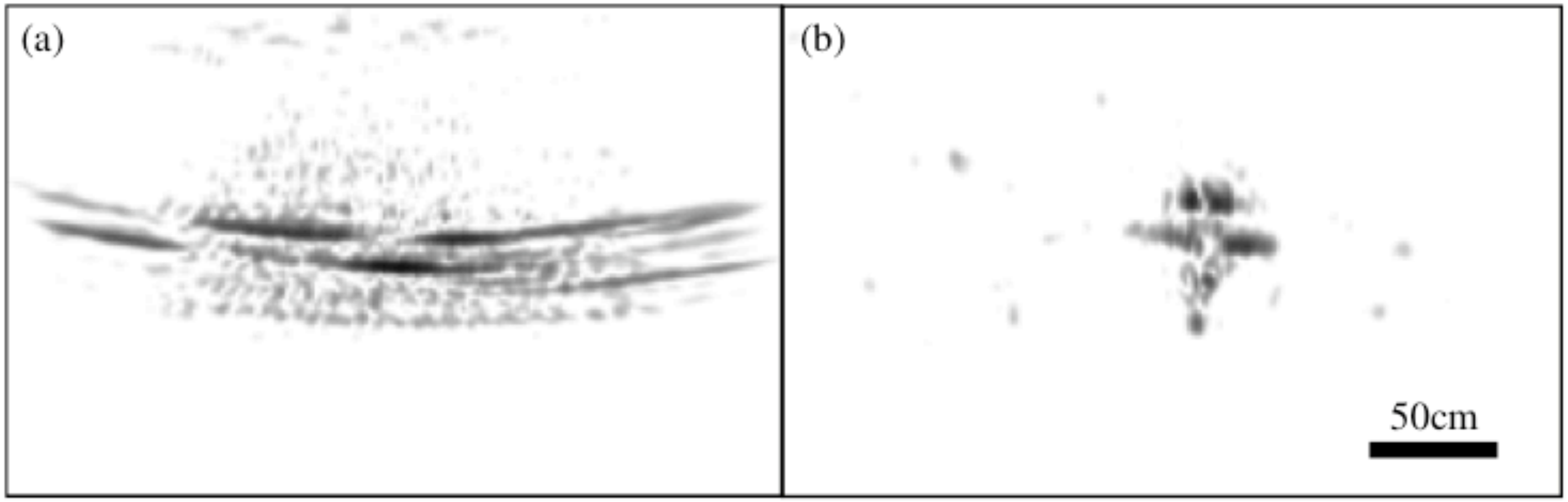

Figure 9. Raw strip-map radar image of a 1:32 scale model of a F14 fighter aircraft before Stolt Fourier resampling (a), and after Stolt Fourier resampling (b).

From Gregory L. Charvat, LIncoln Labs.

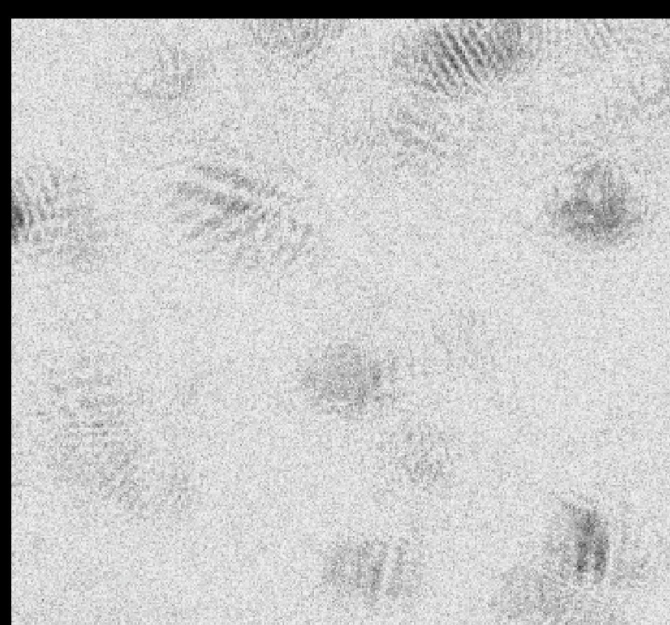

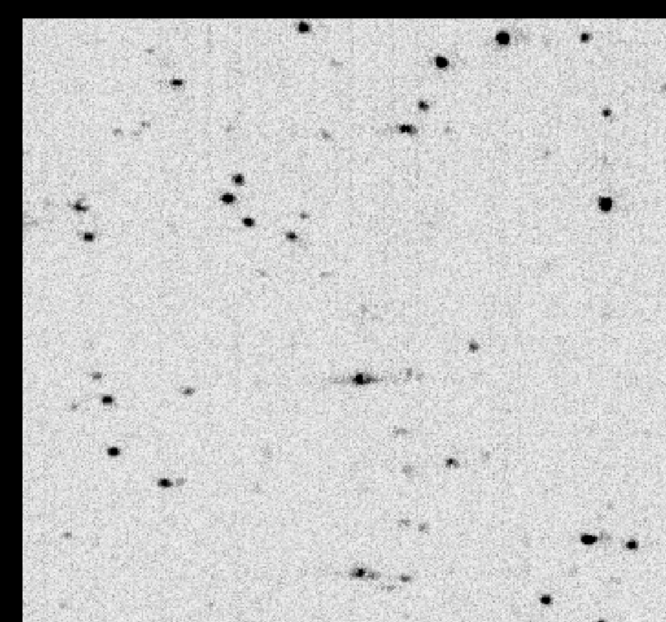

Other bits of magic

- Fast spectral domain acquisition
- Phase drift correction
- Dispersion compensation
- Spectral reweighting

Unstable phase in adjacent planes

Phase fronts

x

in frame

y

across frames

Phase reference

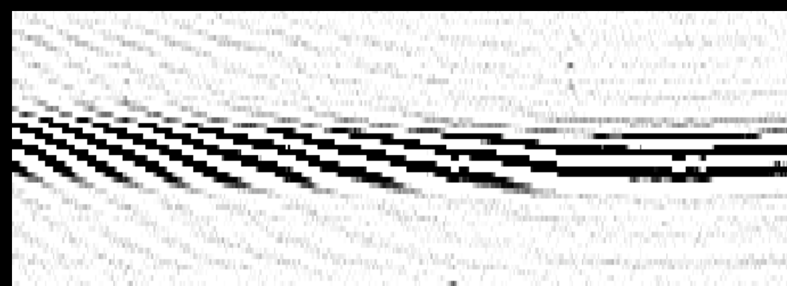

Original Coverslip

Corrected Coverslip

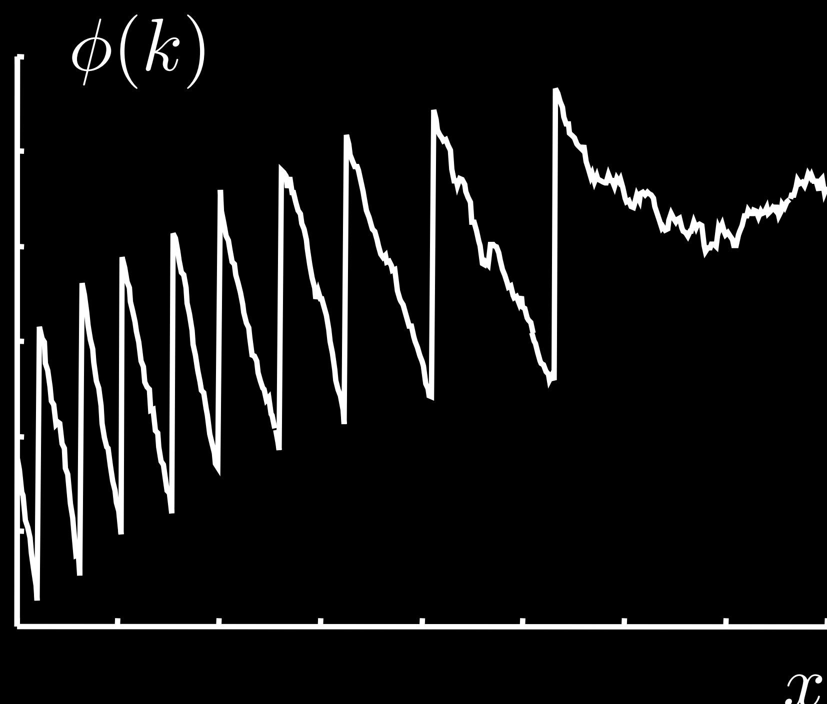

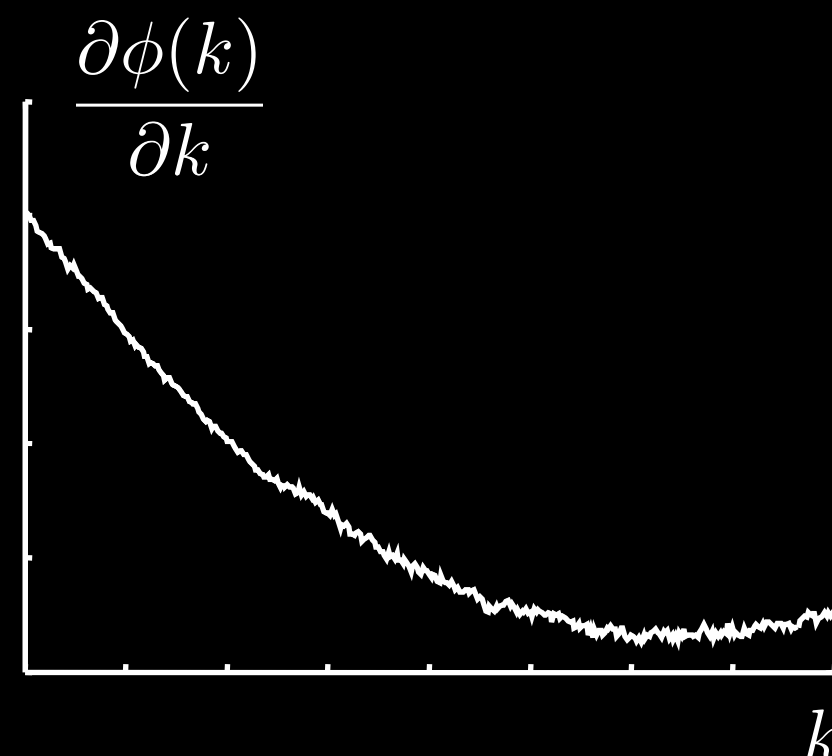

Phase correction using reference coverslip

Phase unstable

Phase corrected

Ralston TS, Marks DL, Carney PS, Boppart SA. “Phase stability technique for inverse scattering in optical coherence tomography.” IEEE International Symposium on Biomedical Imaging, Arlington, VA, April 7, 2006.

Cross-section from a 3D scan

Phase uncorrected

Phase uncorrected reconstruction

Cross-section from a 3D scan

Cross-section from a 3D scan

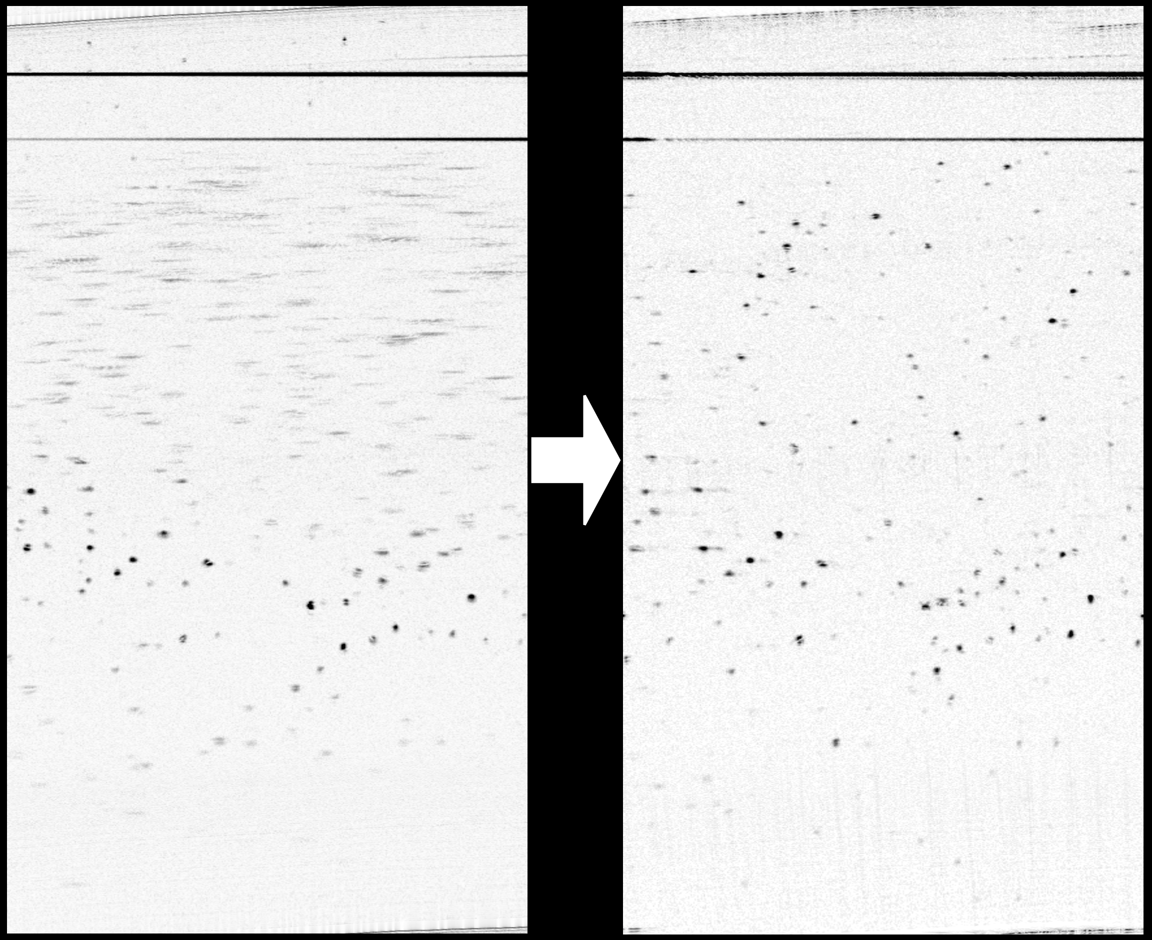

Phase corrected

Phase corrected reconstruction

Spectrum correction in a *Xenopus laevis* (African frog) tadpole

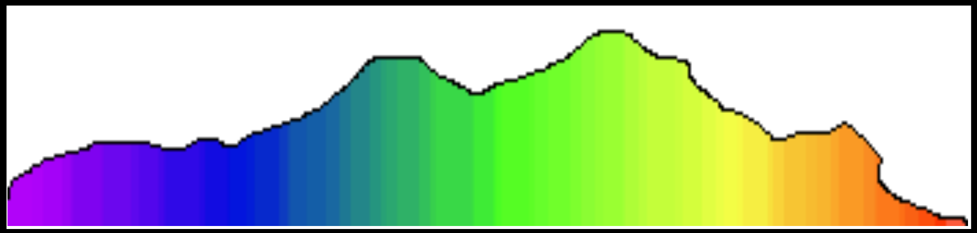

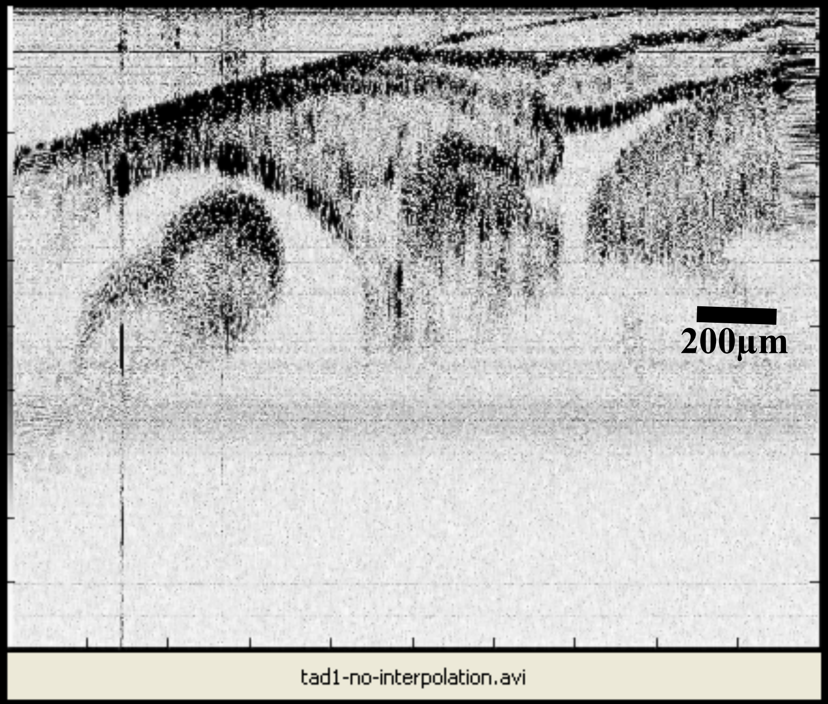

No spectrum correction

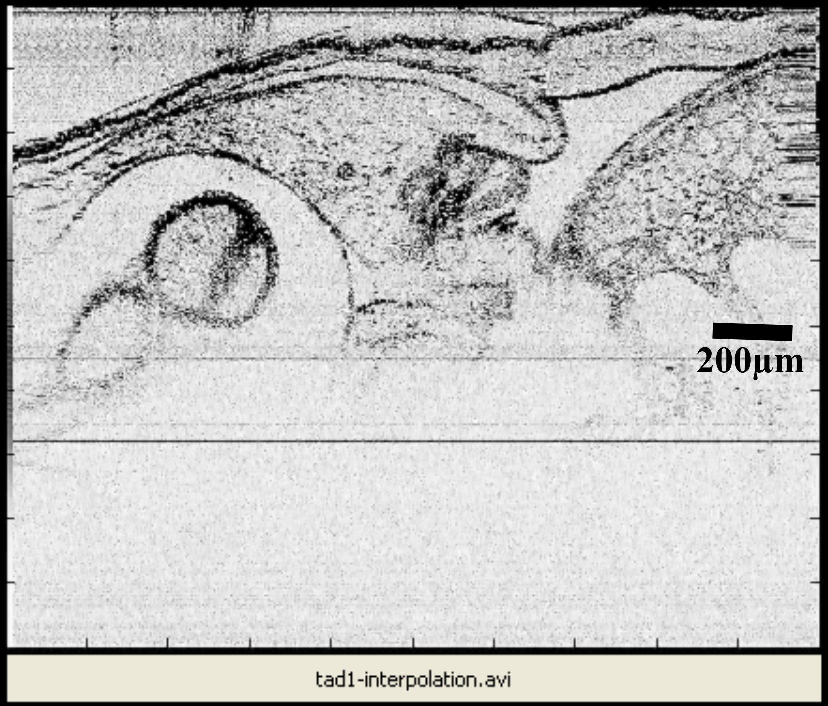

With spectrum correction

Drift (thermal)

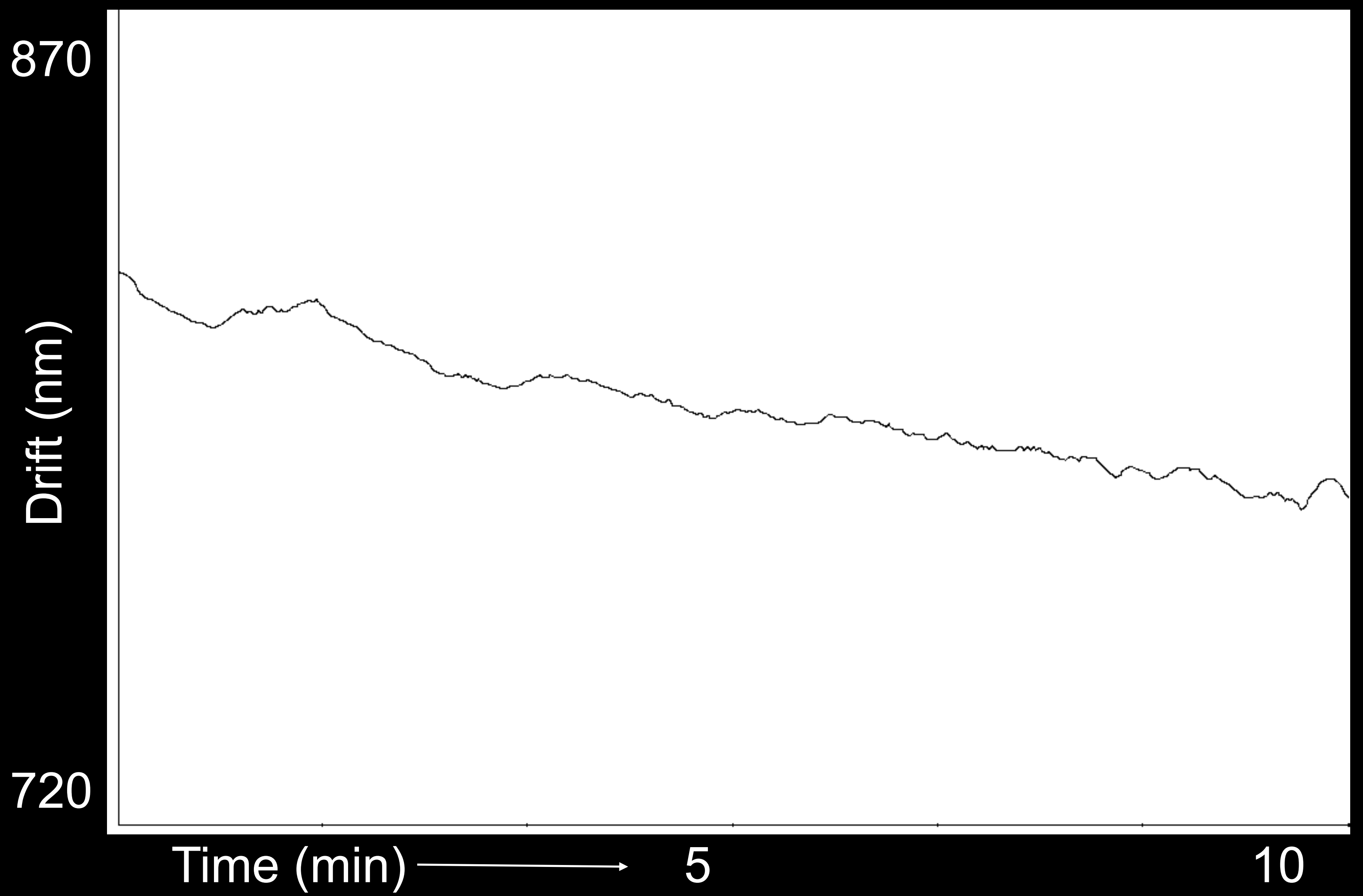

Distorted point response

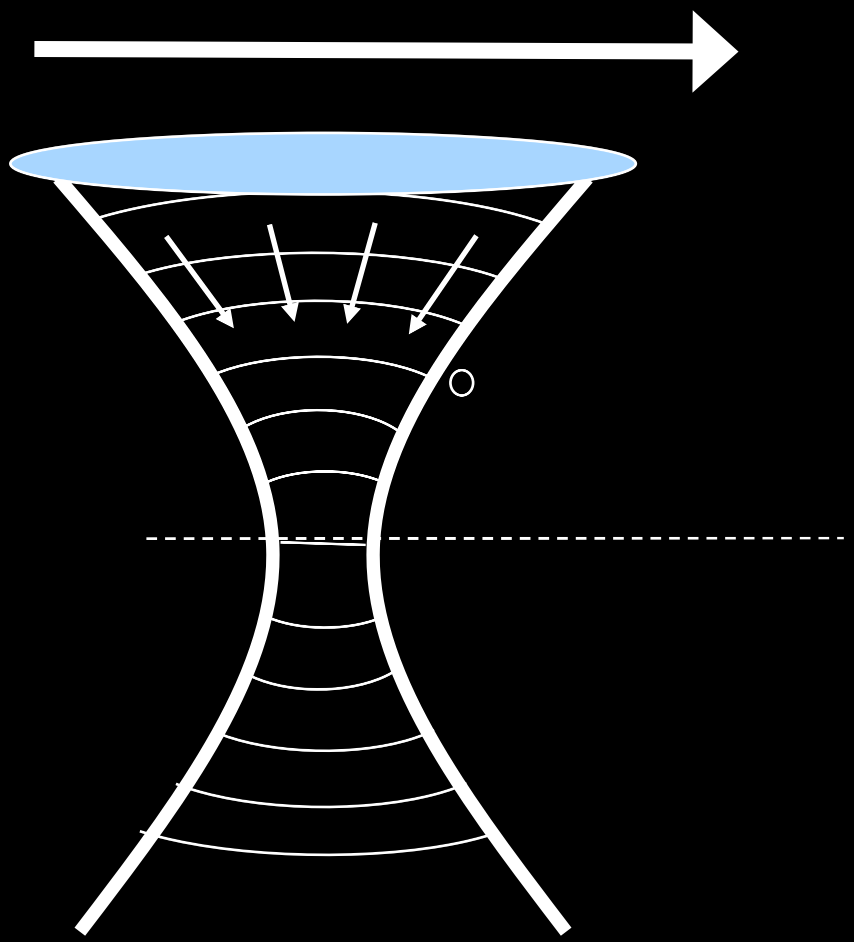

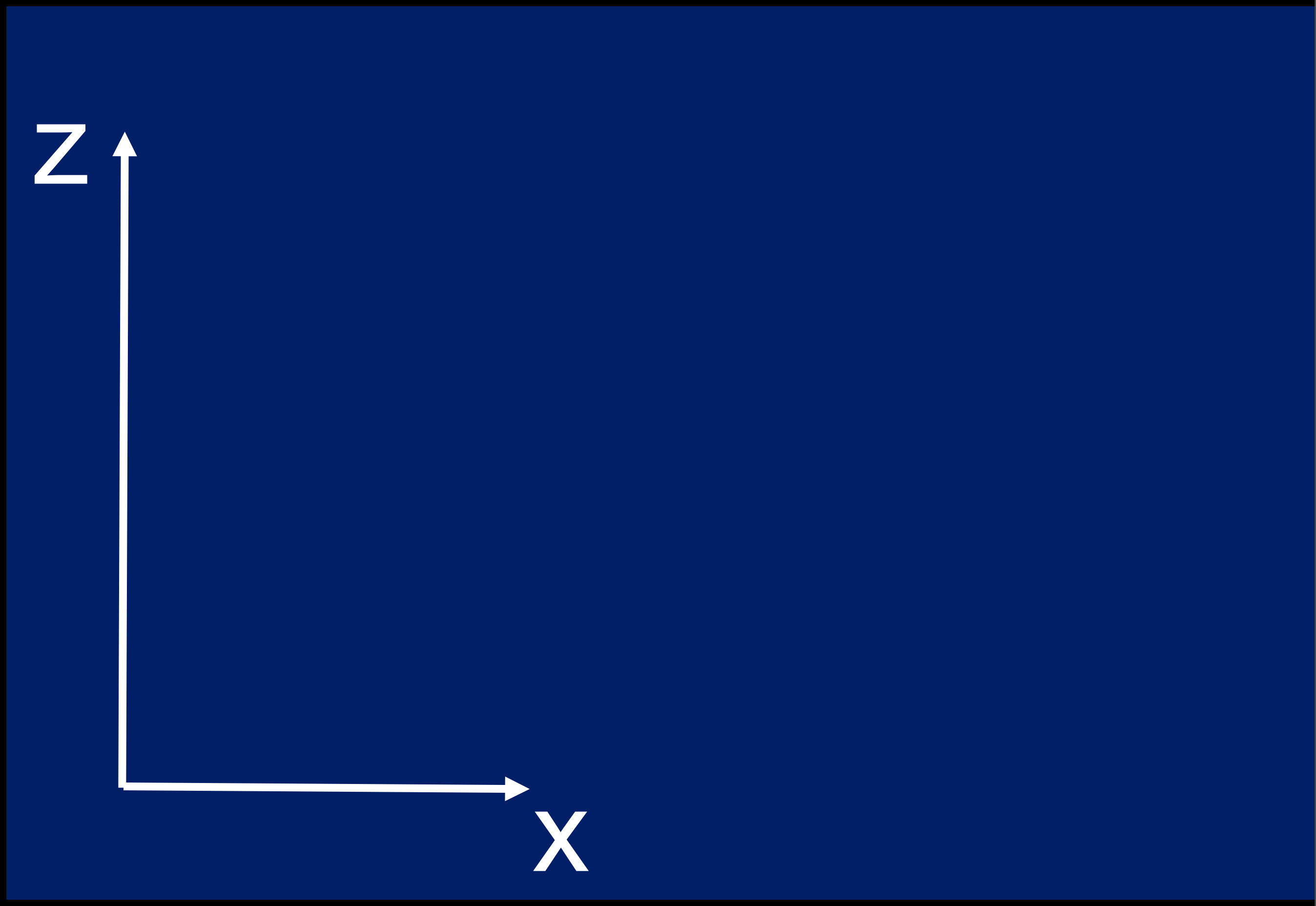

Distorted point response

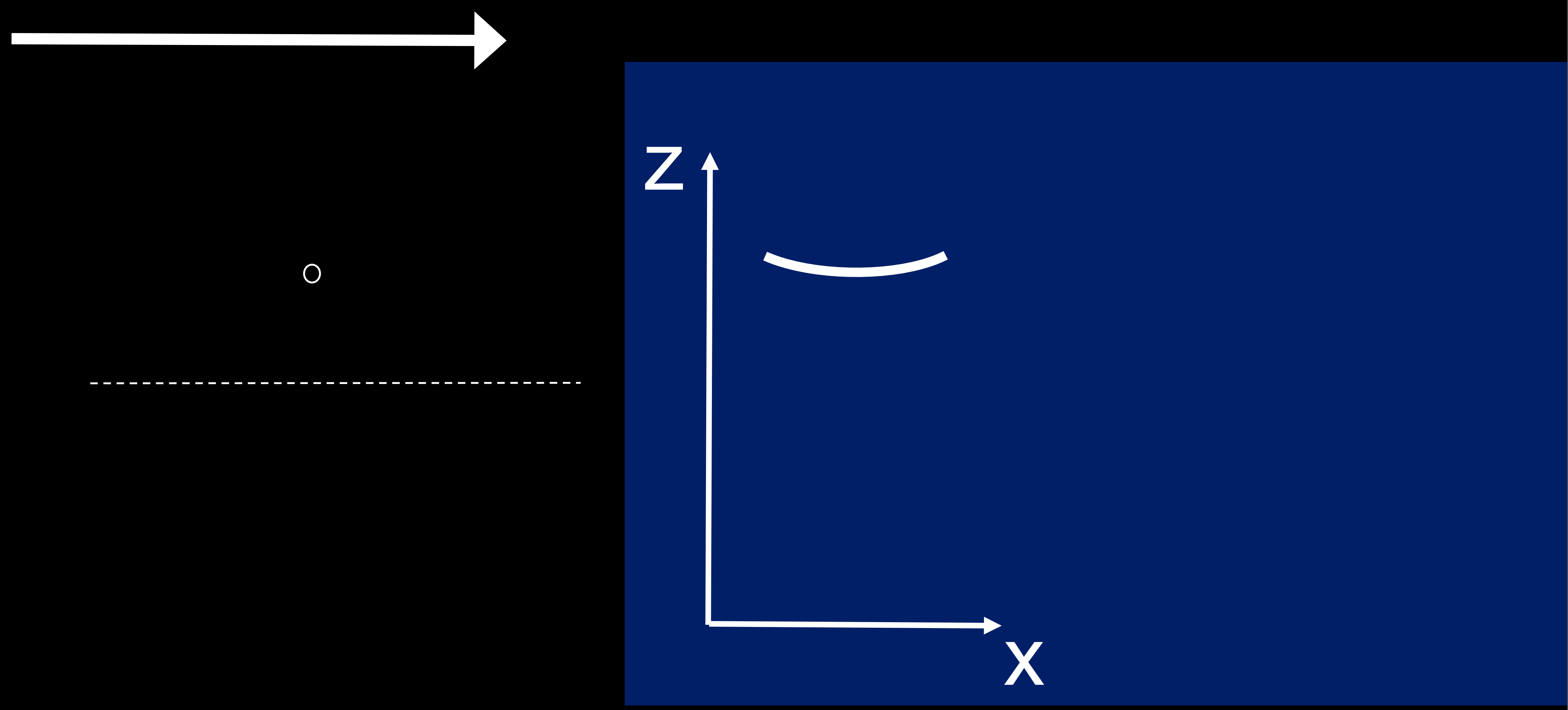

Simulation adjusting the assumed NA

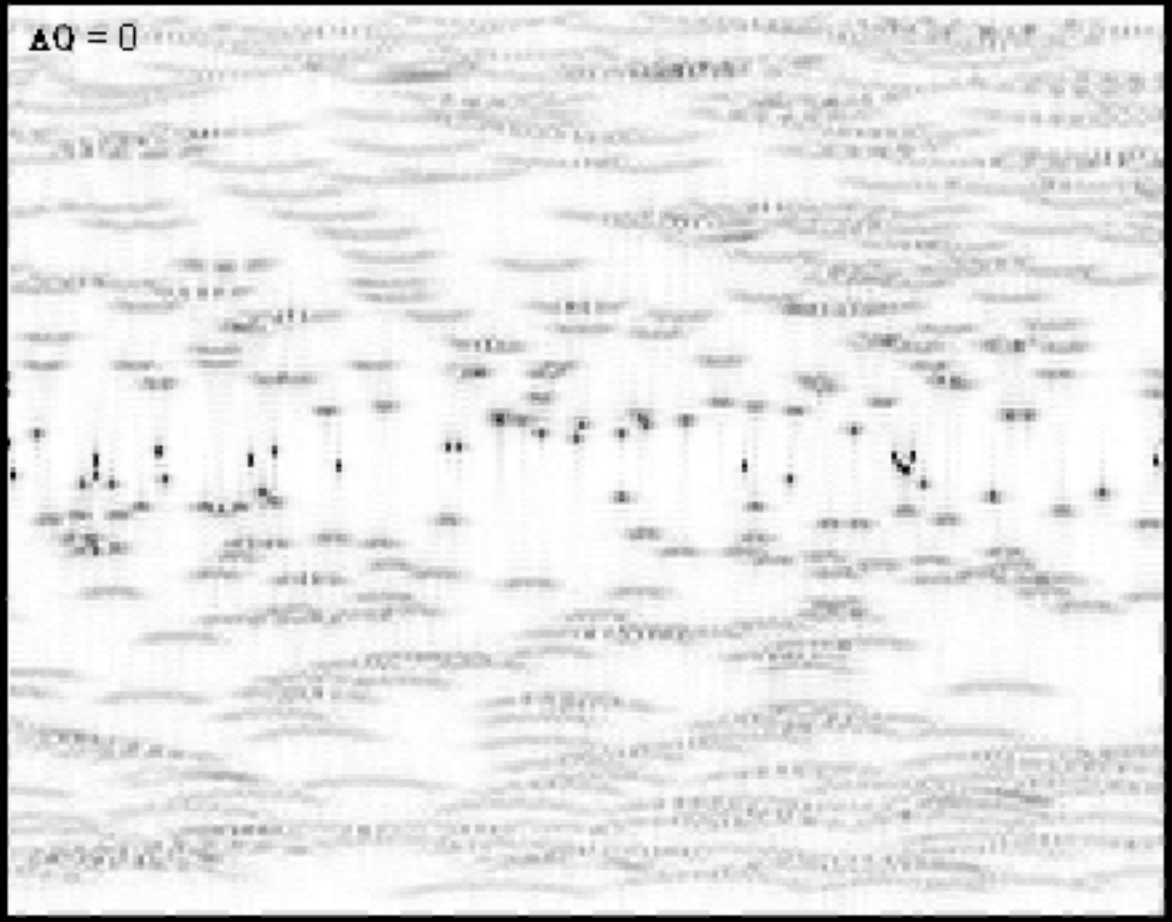

Simulation adjusting the assumed focal plane

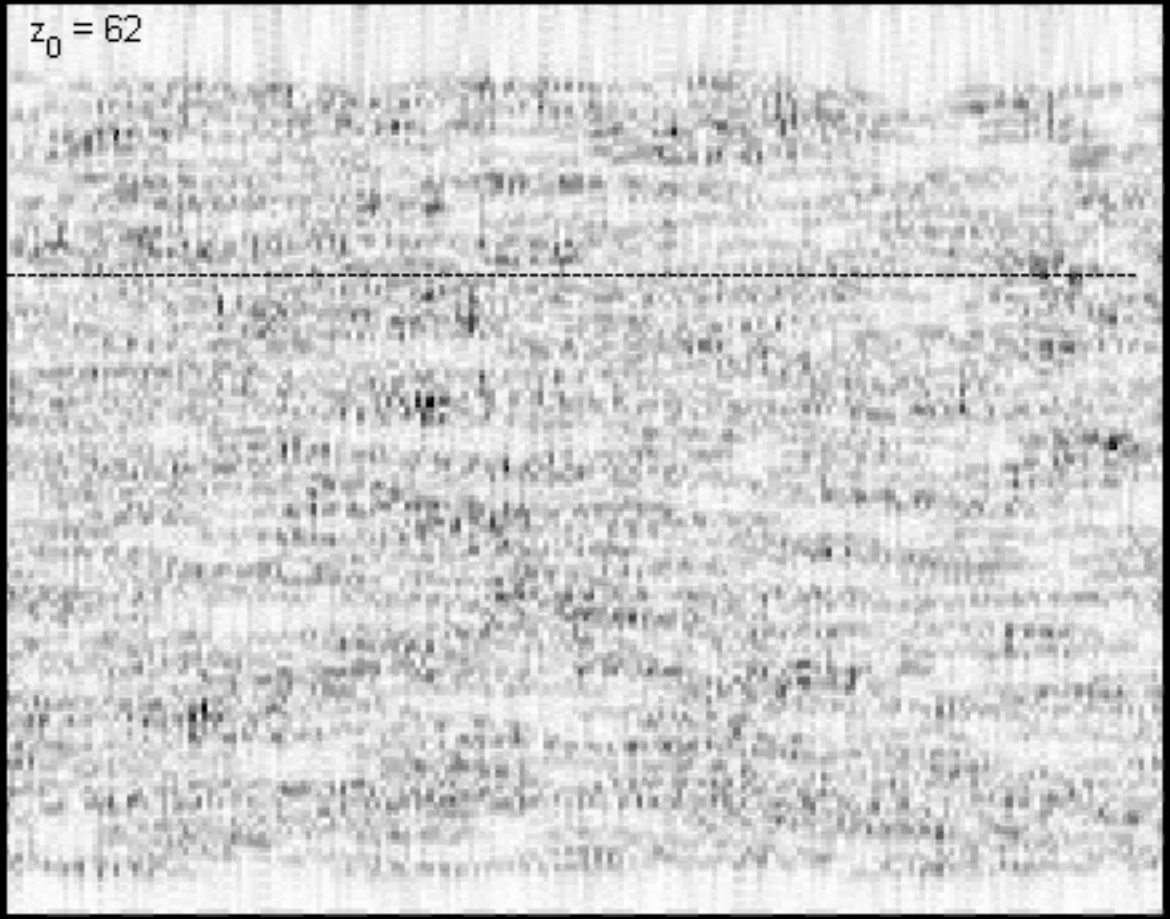

2D projection of 3D scattering

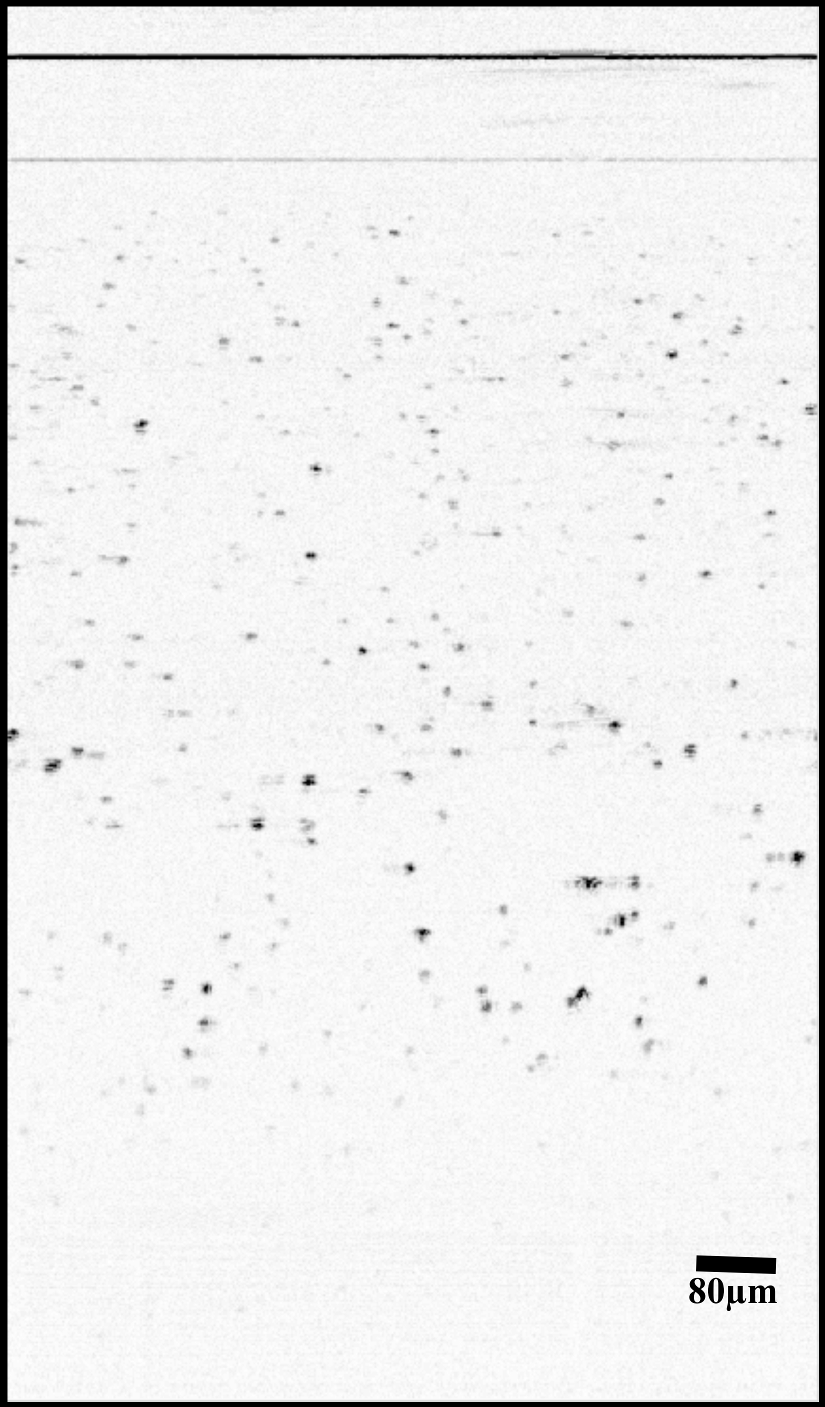

3D beam scattering projected onto $y=y_0$

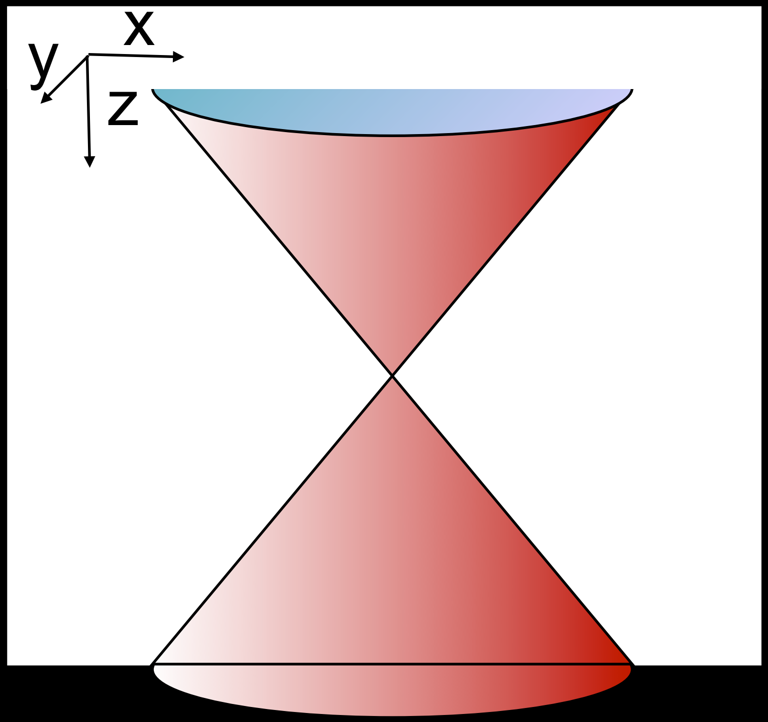

Constant phase surfaces for a point scatterer

$$k_z(\mathbf{q}) = \sqrt{k^2 - q^2}$$

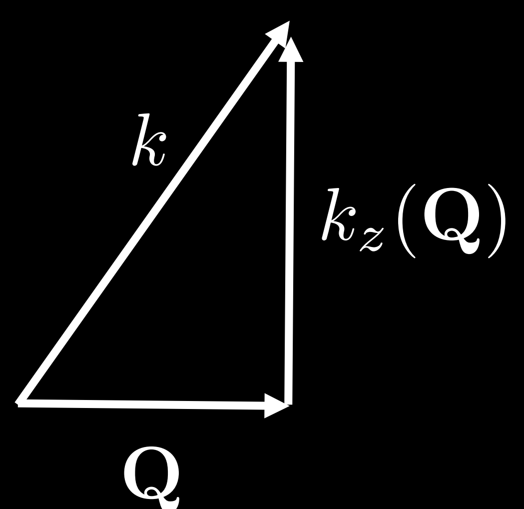

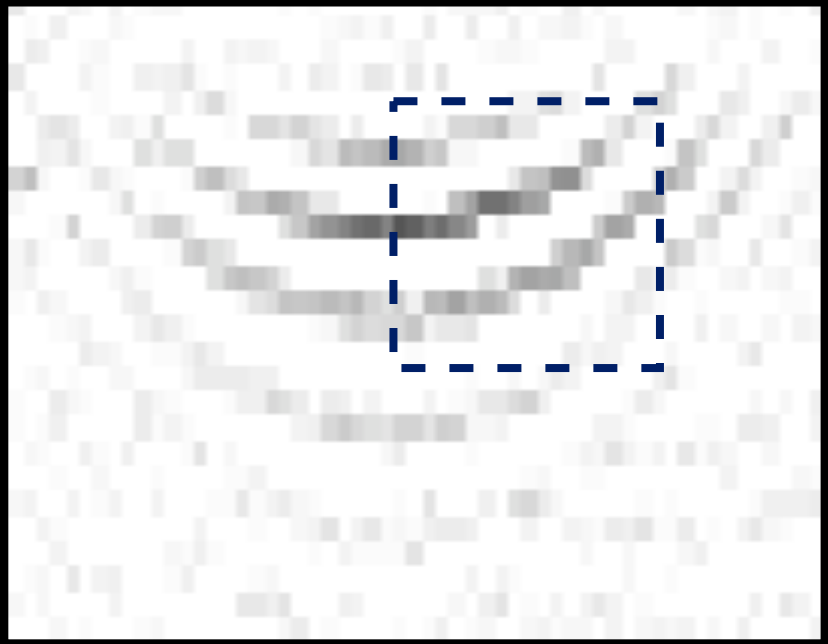

High density sample

2 micron TiO_2 suspended in silicone, SD-OCT

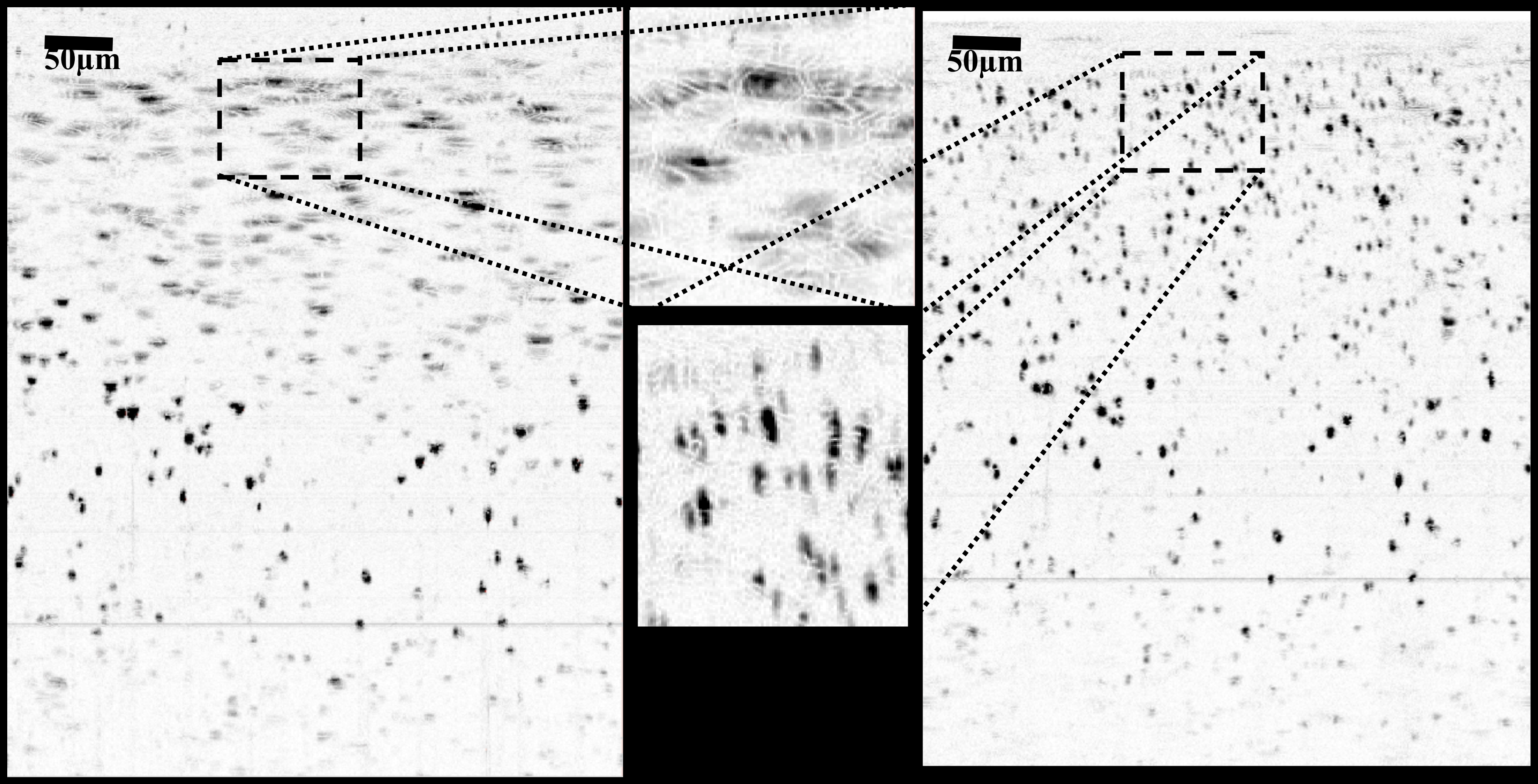

Resampling in the Fourier space

$$\tilde{\tilde{\eta}}(\mathbf{Q},\beta) = \left[\frac{K^*(\mathbf{Q},k,\beta)\tilde{S}(\mathbf{Q},k)}{|K(\mathbf{Q},k,\beta)|^2 + 2Nk/k_z(\mathbf{Q}/2)}\right]_{k=\frac{1}{2}\sqrt{\beta^2-Q^2}}$$

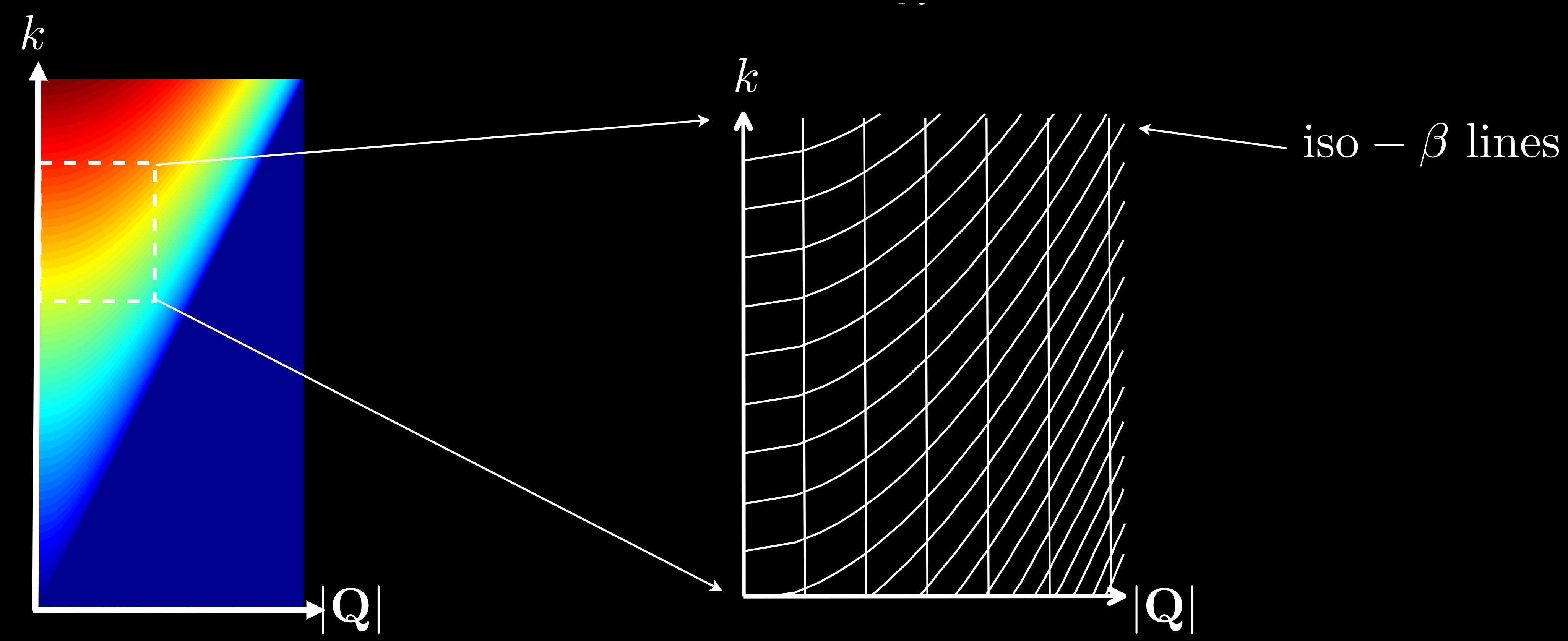

Low Density Experiment

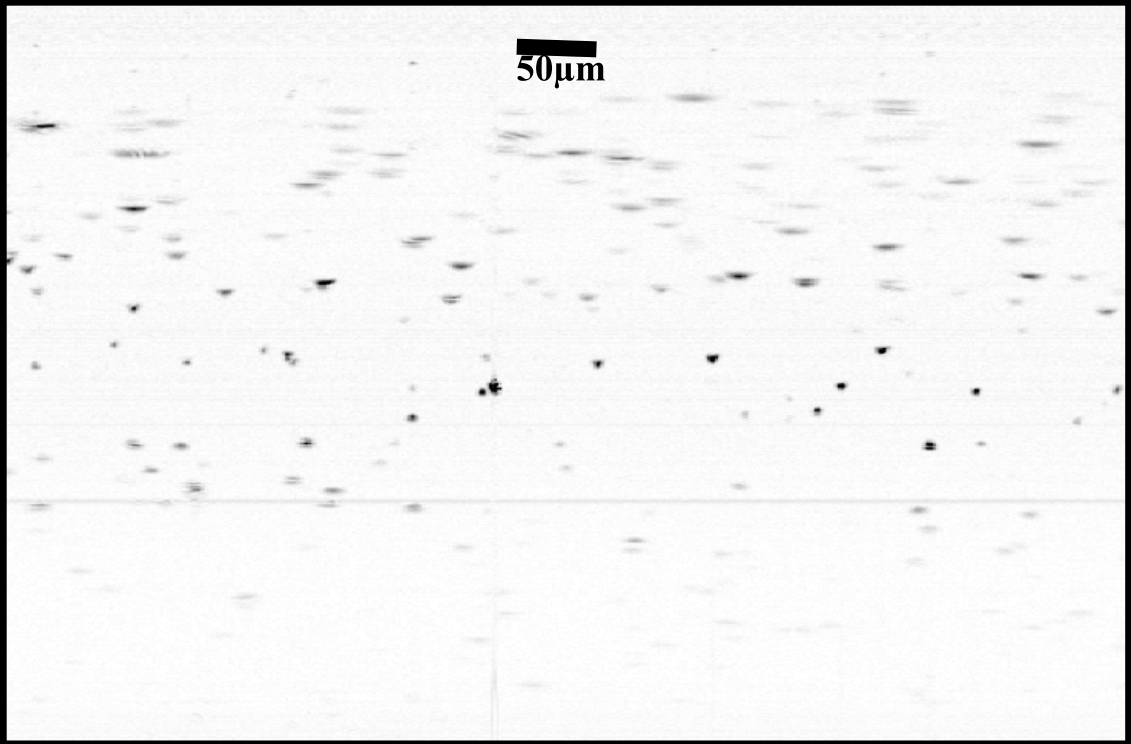

SD-OCT data

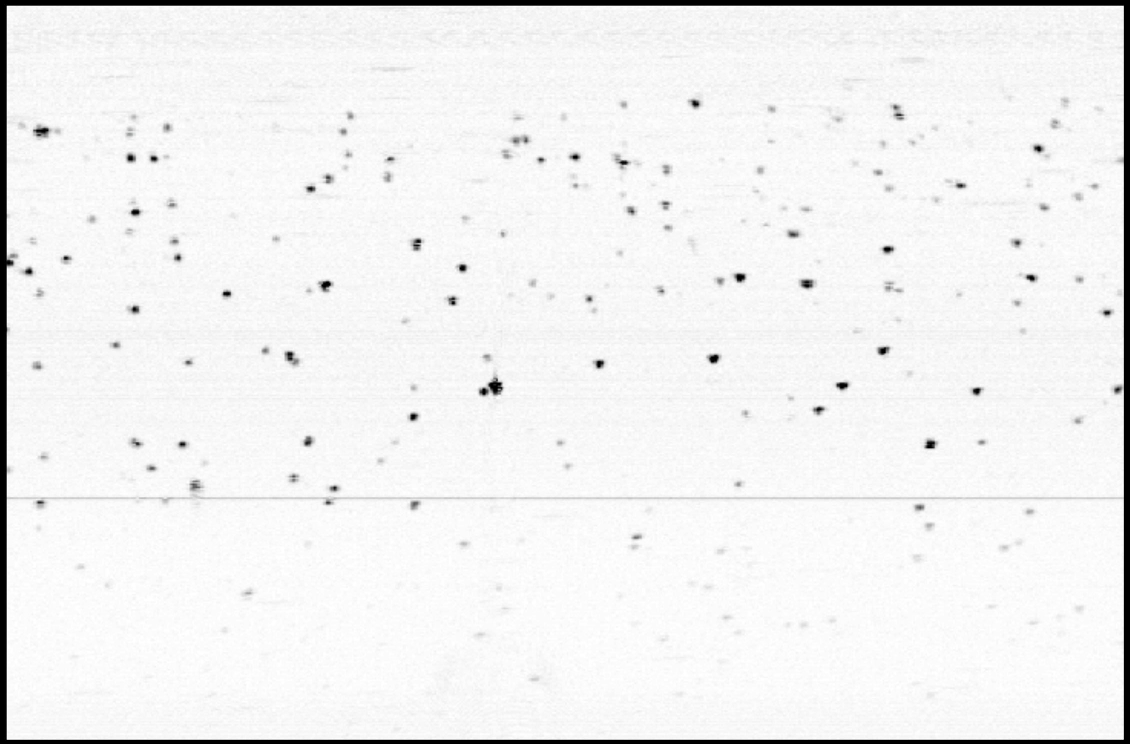

Unfiltered reconstruction

Human Tissue – Adipose/Cancer

ECE Illinois

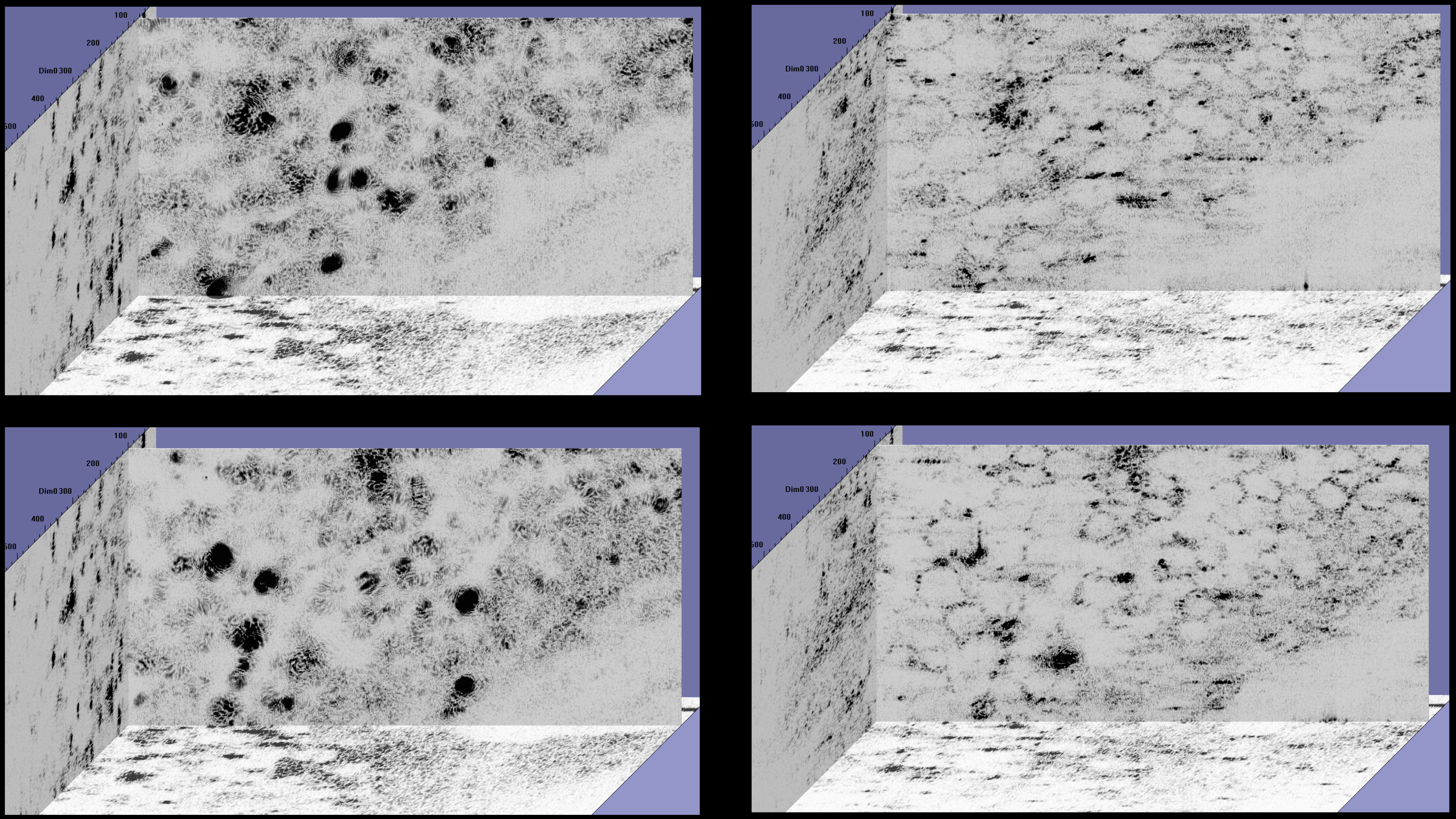

OSG